Chapter 8
Dynamic Analysis of Train-Bridge System Subjected to Collision Loads

In this chapter, the characteristics of various collision loads on bridge are summarized. A dynamic analysis model is established for a coupled high-speed train and bridge system subjected to collision loads. A HSR double-track continuous bridge with (32+48+32) m PC box-girders is considered as an illustrative case study. The dynamic responses of the bridge and the running safety indices of the train on the bridge under three types of collision loads are analyzed. The results show large responses of the bridge induced by collision strongly threaten the running safety of trains. An assessment procedure is proposed for the running safety of high-speed trains on bridges subjected to collision loads, and related threshold curves for train speed versus collision intensity are proposed.

8.1 Collision Loads

When a collision load acts on a bridge pier, it may cause dislocation of bearings and girders, uneven deformation or fracture of expansion joints, and even collapse of girders, resulting in serious accidents, as studied by many researchers (Wuttrich et al. 2001; Larry and Olson 2005; Manuel et al. 2006; Xia et al. 2011; Sharma et al. 2012). For railway bridges, however, even if there is no collapse of girders, the vibrations and displacements induced by collision may deform the track and make it unstable, which may further threaten the running safety of the train on the bridge. When the collision is intense and the train speed is high, the running safety of the train may be seriously affected, and in the most serious case, the train may even derail from the track (Laigaard et al. 1996; Xuan and Zhang 2001; Xia et al. 2012a, b, 2013, 2014, 2015, 2016). As an important part of risk assessment on bridge operation safety, therefore, it is necessary to study the running safety of trains on the bridge subjected to vessel collisions.

Collision is a common physical phenomenon, which is formed by the fast intertouch between two moving objects. The kinetic energy of moving objects is

H. Xia et al., *Dynamic Interaction of Train-Bridge Systems in High-Speed Railways*, Advances in High-speed Rail Technology, https://doi.org/10.1007/978-3-662-54871-4_8

converted into deformation energy during the collision, which is a complex dynamic process. The interacting forces (i.e. the collision loads) formed during the collision process are influenced by many factors, including the mass and velocity of the moving object, the contact area, location and angle of collision, the deformation stiffness of the colliding object itself and the collided structure, and the boundary conditions.

Up to now, a lot of researches have been done toward the collision mechanism between colliding objects and collided bridge structures, based on which some practical design methods for bridge collisions have been proposed, and several related design codes are issued. However, most of the bridge codes adopt the equivalent static analysis method based on simplified static loads, in which the dynamic effects caused by the collision are usually taken into account by various impact coefficients, thus existing a risk of underestimate on the dynamic requirement of the bridge.

In order to study train-bridge coupling vibration and running safety of the train on the bridge subjected to collision loads, it is infeasible to simply use the equivalent static method prescribed in the design codes. However, due to the complexity of the problem, it is very difficult to simultaneously consider the coupling mechanism between the colliding object and the collided bridge structure. An applicable method is to use the time history of collision load as an input of the train-bridge system model to perform the analysis. In this section, some design specifications for bridge collision in Chinese and several foreign codes are introduced, some typical vessel, vehicle and ice-floe collision loads obtained by experiments and FE analysis are concluded, and the characteristics of various collision loads are summarized, which are used to determine the calculation method and to select the intense range of collision loads for the dynamic analysis model of train-bridge system subjected to collision loads in the following sections.

8.1.1 Collision by Vessels

The collision process between a vessel and a bridge structure is very complex, which is related to various factors, such as the circumstances during the collision (storm, climate and flow, and so on), the characteristics of the vessel (the type; size; velocity; loading status of the vessel; and the strength and stiffness of the bow, hull, and deck room), the structural characteristics (geometry, material strength, mass, damping, and stiffness) of the bridge, and the response time of the vessel pilot. Thus, it is very difficult to accurately determine the interacting force between the vessel and the bridge during collision. Over the years, researchers carried out many studies on the mechanism of vessel-structure collision, and according to different physical principles, proposed several practical design formulas for vessel collision loads, and have applied them in the design of bridge piers against vessel collision. These formulas mainly include the following three types.

(1) The design formula for colliding force based on the energy principle. According to the theorem of energy conservation, assuming the initial kinetic energy of the vessel is completely converted into the deformation potential energy after the collision, the maximum collision load can be calculated on account of the deformed stiffness, which is the basis of the Eurocode and the *Fundamental Code for Design on Railway Bridge and Culvert* (TB10002.1 2005) of China. The formula of collision force is established according to the conversion relationship between the kinetic energy and the deformation potential energy of the vessel, in which the factors such as energy loss during collision and colliding angle are considered, and the deformation stiffness is refined as two parts: the vessel stiffness and the bridge-pier stiffness.
(2) The design formula for colliding force based on the momentum principle. According to the momentum principle, knowing the initial momentum and the duration time of the vessel collision, the average collision load can be calculated. In the *General Code for Design of Highway Bridges and Culverts* (JTG D60 2015) of China, the design formula for average collision load adopts this principle, by which the maximum collision load is believed to be two times of the average collision load.
(3) The design formula for colliding force based on the experimental data and experiences. The vessel collision with a pier is a complex nonlinear dynamic process with a huge energy conversion in a very short time. In design codes, the empirical formulas based on simplified static load statistics are usually adopted, such as in AASHTO (1991, 2007), JTG D60 (2015), and TB10002.1 (2005). These empirical formulas, however, cannot take into account the duration time of the collision load, the interaction between vessel and pier, the structural behavior and elastic deformation of the bridge related to the loading rate of collision, etc.

Relatively, experiments are the best way to study the vessel-pier collision, but limited by the high cost and long performing time, full-scale field tests for vessel-pier collision are rarely conducted. Most researches are based on small-scale model tests or swing-hammer impact tests in laboratory, and then, the results are modified according to the accuracy and uncertainties of the test to estimate the actual-scale conditions (Consolazio et al. 2003).

After a half century's efforts, researchers in some countries have developed their respective practical calculation methods for vessel collision loads, and several technical regulations have been proposed in bridge design codes.

The 4th edition of *LRFD Bridge Design Specifications* issued by AASHTO in (2007) prescribes that the equivalent static vessel impact force on bridge pier can be calculated by the following formula

$$F_s = 1.2 \times 10^5 \cdot V_c \cdot \sqrt{\mathrm{DWT}} \tag{8.1}$$

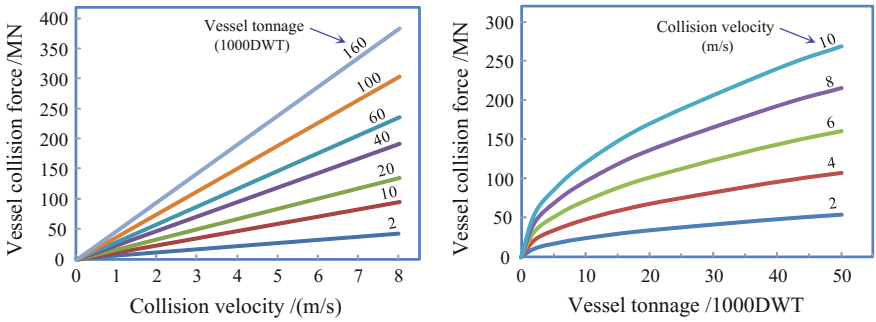

Fig. 8.1 Typical vessel impact forces (AASHTO LRFD)

where F_s is the equivalent static vessel impact force (N); DWT is the deadweight tonnage (Mg) of the vessel (including vessel body, goods, fuel, and water); and V_c is the impact velocity (m/s) of the vessel colliding on the bridge pier.

Shown in Fig. 8.1 are the typical vessel impact forces calculated by Eq. (8.1), with respect to various vessel tonnages and collision velocities

In the *Fundamental Code for Design on Railway Bridge and Culvert* (TB10002.1 2005) issued by the Ministry of Railways of PRC, it is stipulated that the design collision force of vessel to the pier and abutment can be calculated as

$$F = \gamma \cdot V_c \cdot \sin\alpha \sqrt{\frac{W}{C_1 + C_2}} \tag{8.2}$$

where F is collision force (kN); γ is the kinetic energy reduction factor ($s/m^{1/2}$), which can be taken as 0.2 for slanting vessel collision and 0.3 for forward collision; V_c is the vessel speed (m/s) when it collides the pier; α is the angle between the navigation direction of the vessel and the tangent at collision point with the pier; W is the weight of the vessel (kN); C_1 and C_2 are, respectively, elastic deformation coefficients of the vessel and the pier and can be assumed $C_1 + C_2 = 0.0005$ m/kN when lack of data.

The acting position of the vessel collision load should be determined according to the specific condition, and if no related data available, the height of navigable water level can be used.

In Eurocode EN 1991-1-7 and BS EN 1997-1-7 *Actions on Structures, Part 1–7: General Actions—Accidental Actions* (1991, 2006), the vessel collision loads in inland waterway and sea waterway are given for both static design and dynamic design. In this section, only the vessel collision load for dynamic calculation in the Eurocode is introduced.

According to the Eurocode, for the inland waterway vessel, when elastic deformation of the vessel is considered ($E_{def} \leq 0.21$ MN·m), the dynamic design impact force can be calculated by

$$F_{\mathrm{dyn,el}} = 10.95 \times \sqrt{E_{\mathrm{def}}}\,(\mathrm{MN}) \tag{8.3}$$

When the plastic deformation of the vessel is considered ($E_{\mathrm{def}} > 0.21$ MN·m), the dynamic design impact force can be calculated by

$$F_{\mathrm{dyn,pl}} = 5.0 \times \sqrt{1 + 0.128E_{\mathrm{def}}}\,(\mathrm{MN}) \tag{8.4}$$

where the deformation energy E_{def} (MN·m) is equal to the available total kinetic energy $E_{\mathrm{a}} = 0.5\ mV^2$ in case of frontal impact, while in case of lateral impact with $\alpha < 45°$, a sliding impact may be assumed and the deformation energy is taken as

$$E_{\mathrm{def}} = E_{\mathrm{a}}(1 - \cos\alpha) \tag{8.5}$$

In this case, it is recommended to use the average mass m for the relevant vessel type and the design velocity V equal to 3 m/s plus the water flow velocity.

In the dynamic structural analysis, the impact forces should be modeled, according to the response of the vessel, as a half-sine-wave pulse for $F_{\mathrm{dyn}} \leqq 5$ MN (elastic impact) and a trapezoidal pulse for $F_{\mathrm{dyn}} > 5$ MN (plastic impact), with the load durations and other details presented in Fig. 8.2.

For sea-going merchant vessels between 500 DWT and 300,000 DWT, the dynamic design impact force may be determined by

$$F = \begin{cases} F_0\bar{L}\left[\bar{E}_{\mathrm{imp}} + (5.0 - \bar{L})\bar{L}^{1.6}\right]^{0.5} & \left(\bar{E}_{\mathrm{imp}} \geq \bar{L}^{2.6}\right) \\ 2.24F_0\left[\bar{E}_{\mathrm{imp}}\bar{L}\right]^{0.5} & \left(\bar{E}_{\mathrm{imp}} < \bar{L}^{2.6}\right) \end{cases} \tag{8.6}$$

where F is the maximum bow collision force in MN; $\bar{L}$=$L_{\mathrm{pp}}/275$ (m); L_{pp} is the length of vessel in m; F_0 is the reference collision force equal to 210 MN; $\bar{E}_{\mathrm{imp}}$=$E_{\mathrm{imp}}/1425$ (MN · m), E_{imp} is the energy absorbed by plastic deformation, E_{imp}= $0.5\,mV_0^2$ where m is the mass of vessel (10^6 kg), and V_0 is the initial velocity of vessel, taken as 5 m/s.

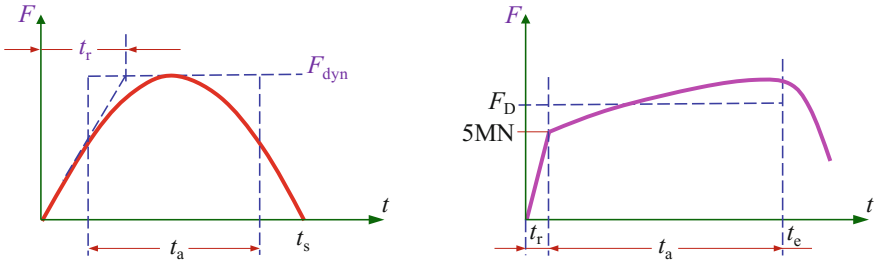

(a) Elastic impact ($F_{\mathrm{dyn}} \leqq 5$ MN) (b) Plastic impact ($F_{\mathrm{dyn}} > 5$ MN)

Fig. 8.2 Load-time functions for vessel collision

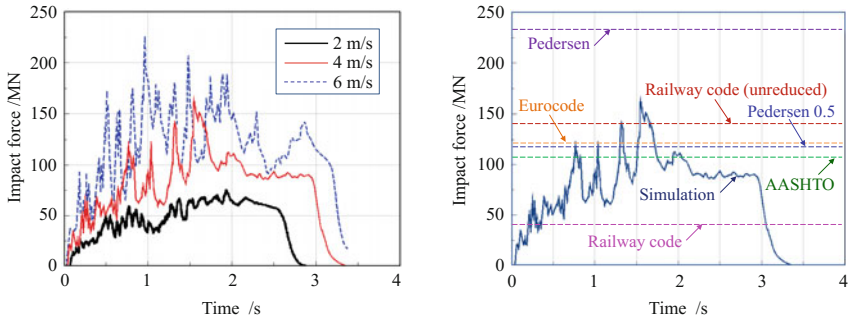

(a) Impact force curves of vessel collision at several velocities (b) Comparison of simplified formula and design codes

Fig. 8.3 Collision force curves of vessel and comparison of simplified formula and design codes

According to the wave propagation theory, the impact load is generated on the interface between the vessel and the bridge, forming a complex dynamic interaction process, which is related to the material and structural characteristics of the vessel and the bridge, and the involved boundary conditions. In this sense, the nonlinear dynamic numerical simulation is a good solution for this problem. With the progress of computer hardware and structural analysis software, the numerical simulation method has been favored by more and more researchers, such as Derucher (1984), Manen (2001), He (2004), Hu et al. (2005), Yan (2006), Wang et al. (2006, 2008), Wang and Chen (2007), Thilakarathna et al. (2010), Fan and Yuan (2012), and many results have been achieved.

Yan (2006) conducted FE simulation analysis on collision of a 50000DWT bulk carrier with several types of pier models, to study the influences of various factors, including vessel velocity (Fig. 8.3a), impact angle, vessel mass, bow stiffness, bow material strain rate and failure strain, and impact contact area and geometry, on the impact force peaks and their occurring time, and loading duration, of collision. By comparing the simulated results with the collision loads from simplified formula and design codes (Fig. 8.3b), he further studied the deficiency of the simplified formula and the applicable conditions of the design collision loads.

Chen (2006) carried out a systematical analysis on the vessel-bridge collision forces, concerning the mass and tonnage of vessel, the impact velocity and angle of collision, the geometry and size of piers and pile caps, and so on. He adopted the LS-DYNA software to simulate the vessel-bridge collision, and obtained several time histories of collision force. Shown in Fig. 8.4a, b are the simulated impact force time histories by collisions of a 5000-DWT bulk carrier with the pier of a (95+3×180+95) m continuous rigid-frame bridge at the speed of 4.0 m/s, and a 3000-DWT one at the speed of 3.0 m/s, respectively.

To better account for dynamic effect of bridge structure under vessel collisions, the equivalent static analysis procedure is employed in most of the design specifications for vessel-bridge collision, but it fails to avoid potentially underestimating the demand.

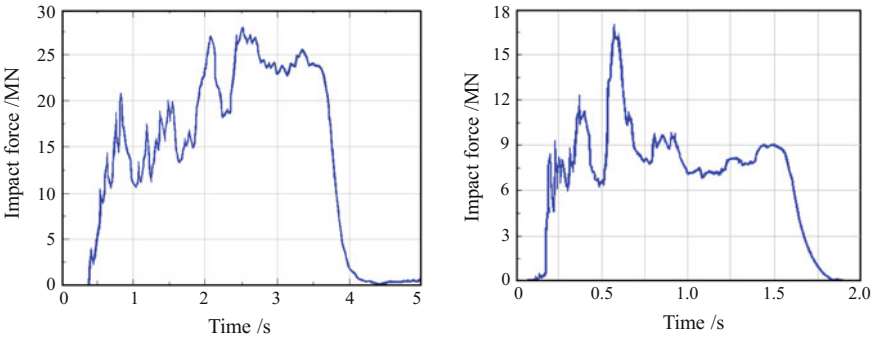

(a) 5000 DWT vessel, V_c=4.0m/s (b) 3000 DWT vessel, V_c=3.0m/s

Fig. 8.4 Collision force time histories of vessels with concrete piers

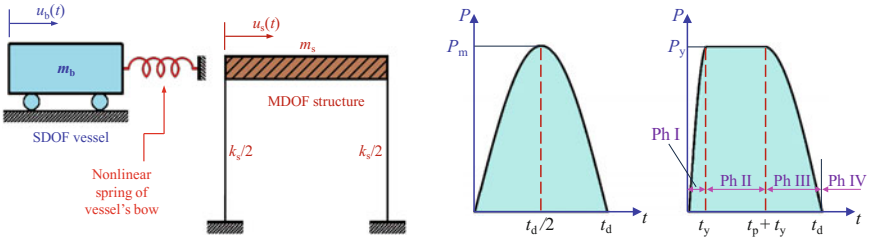

(a) Analysis models (b) Collision force curves

Fig. 8.5 Dynamic system for vessel-bridge collision and typical collision pulse forces

The shock spectrum analysis (SSA) approach was developed based on the theory of vessel-structure interaction in collision, which can efficiently determine the dynamic requirements of bridge structures under vessel collision. By the SSA approach, Fan and Yuan (2012) established a SDOF vessel model and a MDOF structure model, as shown in Fig. 8.5a. Using the models, he simulated the process of bridge subjected to vessel collision and proposed the vessel collision loads for bridge structure.

When the deformation of the bow is at elastic stage during the collision, the vessel-bridge collision force can be expressed as

$$P(t) = P_{\mathrm{m}} \sin(\pi t / t_{\mathrm{d}}) \tag{8.7}$$

where $P_{\mathrm{m}} = V_0 \cdot c_{\mathrm{P}}$ is the deformation energy of the bow; $t_{\mathrm{d}} = \pi m_{\mathrm{b}} V_0 / P_{\mathrm{m}}$ is the total duration time of the collision force; $c_{\mathrm{P}} = (k_{\mathrm{e}} \cdot m_{\mathrm{b}})^{1/2}$ is defined as the pseudo-damping coefficient; and k_{e} is the effective spring stiffness of the vessel-bridge collision.

When the deformation of the bow is at plastic stage during the collision, the vessel-bridge collision force can be expressed as

$$P(t) = \begin{cases} P_y \sin(\omega_y t) & (0 \le t < t_y) \\ P_y & (t_y \le t < t + t_y) \\ P_y \sin[\omega_u (t - t_d + 2t_u)] & (t_p + t_y \le t - t_d) \end{cases} \tag{8.8}$$

where $\omega_y = \pi/2t_y$, $\omega_u = \pi/2t_u$, and $t_u = \pi m_b/(2c_p)$.

Shown in Fig. 8.5b is the typical vessel collision force curve obtained by Eq. (8.8). It can be found that the collision load given in the figure is consistent with the dynamic analysis loads in EN 1991-1-7 of Eurocode and BS EN 1997-1-7 issued by the UK.

Chen et al. (2008) established a 3-D FE model to simulate and calculate the collision process between an oil tanker vessel with the weight of 1900 DWT and the tower platform of a long-span rail-cum-road cable-stayed bridge, by using the parallel computing technology based on the contact equilibrium, and obtained the time history of collision force, as shown in Fig. 8.6. It can be seen that during the collision, the collision force increases firstly, and reaches the maximum value of 11.2 MN at 0.63 s, then decreases gradually and reduces to zero at about 1.4 s when the vessel is rebound from the tower cap. The fluctuation of the collision force indicates several loading and unloading of the vessel structure during the collision process, and each unloading represents a failure or damage of a certain bow structure.

The anti-collision design is an important issue for bridge against vessel impact. He (2008) simulated the process of a 50000-DWT bulk carrier colliding on a bridge pier at velocity of 4.0 m/s and obtained the time histories of impact force considering the pier with and without anti-collision device, as shown in Fig. 8.7.

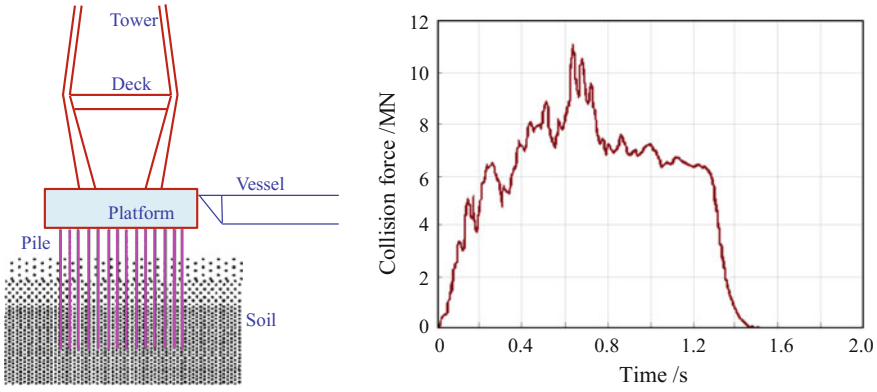

Fig. 8.6 Analysis model for vessel-tower-cap collision and impact force time history (1900DWT oil tanker vessel, V_c = 4.12 m/s)

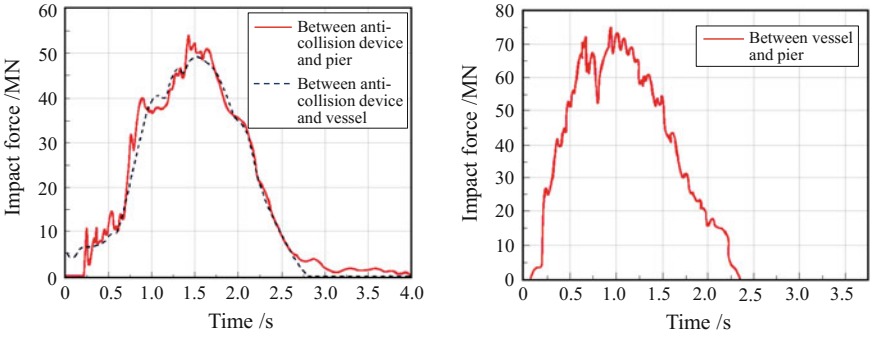

(a) With anti-collision device (b) Without anti-collision device

Fig. 8.7 Impact force time histories of a 50000DWT bulk carrier (V_c = 4.0 m/s)

According to the results, for the pier with anti-collision device, the vessel collision load shows a long duration of about 4.0 s, with the maximum impact force of 55 MN. While for the pier without anti-collision device, the collision load shows a shorter duration of about 2.5 s, but a greater maximum impact force of 75 MN, increased by 35% of the former.

The collision force curves exhibit jumped changes at several collision phases, indicating a strong nonlinear wave characteristic, which shows the anti-collision device effectively involved in the protection work, or reflect the failure or damage of structural components. This nonlinear wave characteristic is also found in other studies, such as those in Luo (2008) by simulation of a 1000 t vessel colliding on the pier with the anti-collision device at velocity 5 m/s, and in Li et al. (2006) by a 5000 t vessel colliding on the anti-collision device of the pier at 2 m/s.

The maximum impact force of vessel collision on pier is one of the most important factors for a bridge design. By means of nonlinear finite element simulation method, Hu et al. (2005) calculated the impact forces of collision between bow and rigid bridge pier for vessels of 5,000 ~ 60,000DWT and obtained the curves of maximum collision force versus vessel tonnage at several collision velocities, as shown in Fig. 8.8.

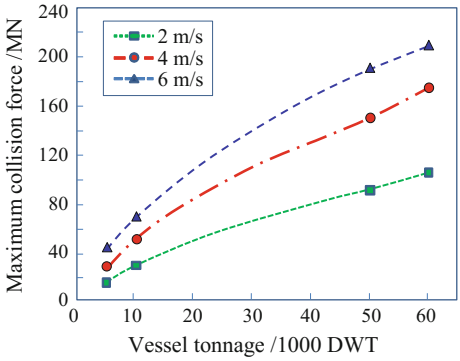

Fig. 8.8 Maximum collision forces of vessel with different DWTs

These research results show that the collision loads of vessel with pier are very complex. In general, the time histories of impact forces exhibit a characteristic of strong nonlinear waveform, with loading duration of about 3 $\sim$ 4 s; the heavier the vessel, and the faster the impact velocity, the greater the instant collision force, with the maximum being hundreds of MN.

8.1.2 Collision by Road Vehicles

Compared with the vessel and ice-floe collisions on bridge structures, the collision of road vehicle on bridge is more often. In a collision accident, with the vehicle crush, the bridge may be damaged or even collapsed due to the intense and sudden impact, bringing even more serious casualties and property losses. As indicated by researches and some related codes, vehicle-collision loads are very complicated, and the values of collision force are quite different for the various vehicle types under different conditions, such as the weight and velocity of vehicle, and the impact position and angle of collision.

In some countries, the vehicle collision is regarded as one of the most likely accidental loads for bridge structures, and related criteria for vehicle collision forces are set in design codes.

In the 4th edition of *LRFD Bridge Design Specifications* issued by AASHTO in (2007), it is prescribed that the bridge pier located within a distance of 9.0 m to the roadway edge or 15.0 m to the center line of a railway track shall be designed for an equivalent static force of 1,800 kN, which is assumed to act in any direction, in a horizontal plane at 1.2 m height above the ground.

In China, the design codes for roadway bridge (JTG D60 2015), railway bridge (TB10002.1 2005), and HSR bridge (TB10621-2014 2015) prescribe that: In case that pier columns are likely to be bumped by cars, if without protection works, the impact force shall be considered as 1,000 kN along the traffic direction, and 500 kN across the traffic direction, horizontally acting on the pier at 1.2 m above the road surface. The collision forces in two directions shall not be considered together.

In Eurocode EN 1991-1-7 and BS EN 1997-1-7 *Actions on Structures, Part 1–7: General Actions—Accidental Actions* (European Standard 1991, 2006), design values for actions due to impact on the columns of bridges adjacent to roads and railways are defined. The indicative equivalent static design forces due to vehicular impact are 1,000 kN in travel direction and 500 kN perpendicular to travel direction, horizontally acting at 0.50 m (cars) to 1.50 m (lorries) level above the surrounding ground surface or higher where certain types of protective barriers are provided. The indicative equivalent static design forces due to the impact of derailed train are 4,000 kN along the track direction and 1,500 kN perpendicular to the track direction, horizontally acting at 1.8 m above the track level. When the train speed is greater than 120 km/h, a risk analysis should be carried out by using refined methods such as dynamic analyses, nonlinear models, and interaction between the load and the structure. In the absence of a dynamic analysis, the

dynamic amplification factor for the elastic response may be assumed to be equal to 1.4.

The impact is characterized as either *hard impact*, where the energy is mainly dissipated by the impacting body, or *soft impact*, where the structure is designed to deform in order to absorb the impact energy.

For hard impact, it is assumed that the structure is rigid and immovable and that the colliding object deforms linearly during the impact phase. The maximum dynamic interaction force is given by expression

$$F = V_c\sqrt{k \cdot m} \tag{8.9}$$

where V_c is the velocity of the object when impacting; k is the equivalent elastic stiffness of the object (i.e., the ratio between force and total deformation); and m is the mass of the colliding object.

In this case, the force due to impact may be considered as a rectangular pulse on the surface of the structure, as shown in Fig. 8.9, and the duration of the pulse follows from

$$F\Delta t = mV_c \qquad \text{or} \qquad \Delta t = \sqrt{m/k} \tag{8.10}$$

in which $k = EA/L$ and $m = \rho AL$, when the colliding object is modeled as an equivalent impacting object of uniform cross section (see Fig. 8.9); L, A, E, and ρ are, respectively, the length, cross-sectional area, modulus of elasticity, and mass density of the colliding object.

If the structure is elastic and the colliding object is rigid, the collision energy is mainly absorbed by the deformation of the structure, and it can be regarded as "soft collision." Equations (8.9) and (8.10) are still applicable, while they should be used with k being the stiffness of the collided structure.

Generally, there are two ways to acquire the dynamic collision loads: on-site experiment and mathematic simulation. In studying truck collision with bridge pier, the full-scale test is very costly, because the expensive truck will be completely destroyed after impact, while the small-scale model test can hardly provide the required impact force curves, therefore, most investigations are based on finite element simulation (EL-Tawil et al. 2005; Buth 2009; NCAC 2010; Sharma et al. 2012). Buth (2009) established a FE model to simulate the complex process of a

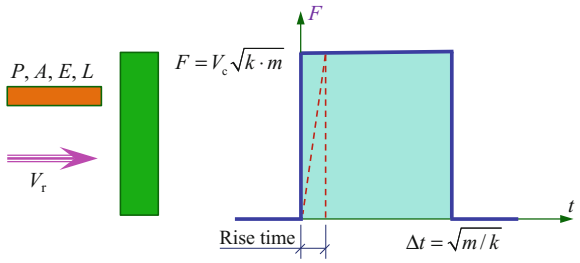

Fig. 8.9 Impact model (Eurocode)

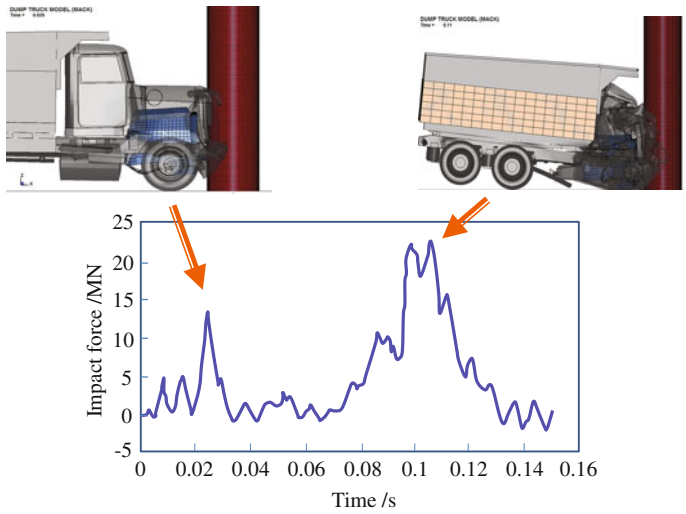

Fig. 8.10 Impact force time histories of a dump truck collision with pier

truck crash with an RC column of a bridge over the I-20 highway in Texas in the USA. He captured the time histories of collision force between the truck and the column and reported a general agreement between the simulated crack pattern and the actually observed failure mechanism of the column. The time history given in the Fig. 8.10 is the collision load of a 289-kN-weight dump truck colliding on the bridge pier with the velocity of 96.6 km/h, and the figure also shows that the states of truck and bridge pier after collision are related to the two peaks in the curve.

The impact force time history is formed by the interacting response of colliding truck and the collided pier. Owing to the structural and mass distribution characteristics of the truck, there appear two main peaks in the curve of Fig. 8.10. According to some researches, the durations of collision loads in various cases are basically the same.

The impact force by truck collision is usually measured by the "50 ms moving average" value. Shown in Fig. 8.11a are the impact force curves simulated with the 289-kN dump truck at two impact velocities (Buth 2009). It can be seen that the variation of the impact force curves is relatively less fluctuated. The maximum values of the impact force curves after "50 ms moving average" are often taken as the design load.

Similar results are presented by Yu and Zha (2011), who established a dynamic model to investigate the impact of a truck with a bridge pier. The truck had a weight of 77 kN, and the FE model of the truck was the one issued by NCAC (National Crash Analysis Center 2010) in the USA. Shown in Fig. 8.11b are the "50 ms

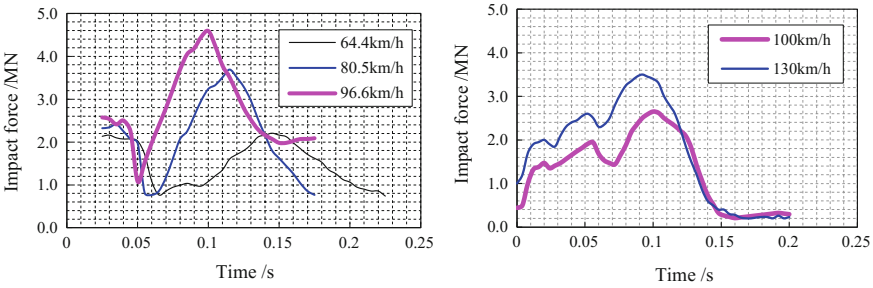

(a) 289 kN dump truck (b) 77kN truck

Fig. 8.11 Impact force time histories of truck collision with piers after "50 ms moving average"

moving" averaged collision force time histories of the truck acting on the pier at two impact velocities V_c = 100 km/h and V_c = 130 km/h, and the corresponding peak forces are 2.65 MN and 3.5 MN, respectively.

El-Tawil et al. (2005) used the inelastic transient finite element method to simulate the collision forces between truck and bridge pier. A 14 kN-Chevy truck and a 66 kN-Ford truck and two types of concrete piers were used in the simulation, and the impact velocities for the trucks were from 55 to 135 km/h. Shown in Fig. 8.12 are the impact force time histories of truck collision with pier.

These time histories of impact forces show a characteristic of narrow pulse load with very short loading duration of about 0.1 s and the pulse width of 0.003 s ~ 0.01 s; the faster the vehicle velocity, the earlier the peak appears, and the narrower the pulse width.

Regarding the collision intensity, El-Tawil et al. further studied the distributions of peak dynamic force (PDF) and equivalent static force (ESF, the static force necessary to produce the same displacement as that produced by the dynamic force) of the two trucks versus approach velocity, as shown in Fig. 8.13, where the design loads in AASHTO and Chinese code are also given for comparison.

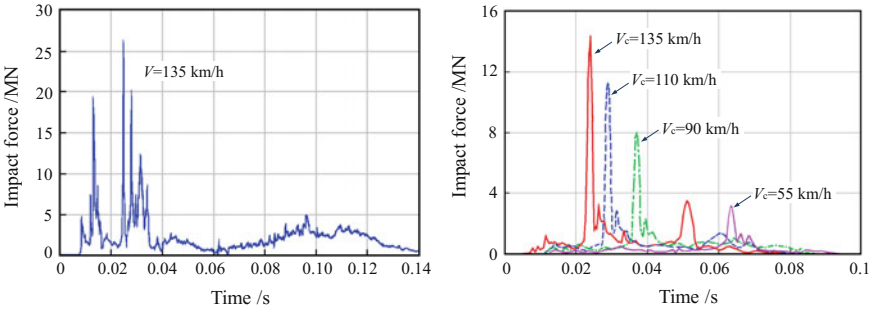

(a) 66 kN-Ford truck (b) 14 kN-Chevy truck

Fig. 8.12 Impact force time histories of truck collision with pier (El-Tawil et al. 2005)

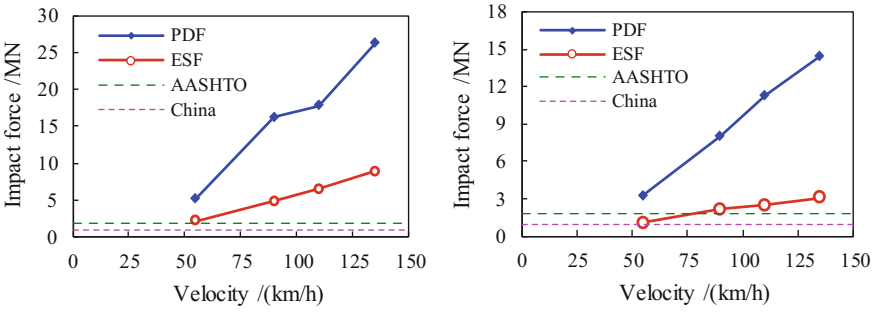

(a) 66 kN-Ford truck (b) 14 kN-Chevy truck

Fig. 8.13 Distributions of truck impact forces versus approach speed

The results showed that the collision forces appear to increase rapidly with the approach velocity of the truck. The maximum PDF is as high as 26.3 MN for the Ford truck and 14.4 MN for the Chevy, and the maximum ESF is 8.85 MN for the Ford and 3.07 MN for the Chevy, respectively. Even for the ESF, it turns out to be significantly higher than the design values (1.8 MN in AASHITO and 1.0 MN in Chinese code) when the truck velocity is high, indicating that the current collision design provisions could be severely insufficient and that there might be a number of bridge piers vulnerable to accidental impact of heavy trucks. Moreover, it should be mentioned that as the freight trucks are often overloaded and sometimes over-speeded in China, the actual collision forces might also be much greater than the one provided in the code.

Based on the refined nonlinear finite element analysis and the accident case investigation, Lu et al. (2011) studied the impact force and the structure damage mechanism of overheight truck colliding with bridge superstructures. Illustrated in Fig. 8.14a are the calculated impact force time histories of a 2-axle truck colliding with the T-beam of a bridge at several velocities. The curves show that the collision loads are greatly affected by the mass and the colliding velocity of truck, and both lateral and vertical impact impulses have linear relationship with the velocity of the truck, while they are little affected by the type of bridge structure (Fig. 8.14b).

Subsequently, further studies by Lu et al. (2011) and Xu et al. (2012, 2013) found that collision between overheight truck and bridge superstructure causes two types of failure modes, viz global damage and local damage, which are necessary to be incorporated into the bridge design. To reduce computation cost and facilitate engineering application, a simplified model for calculating the collision forces is proposed. The collision force histories by the simplified model and the FE method are compared in Fig. 8.15.

Sharma et al. (2012) developed a framework for estimating the dynamic shear force capacity of an RC column subjected to vehicle collision for different performance levels of the design. The method, as a more realistic representation of vehicle collision with structures, is an improvement over the existing static or

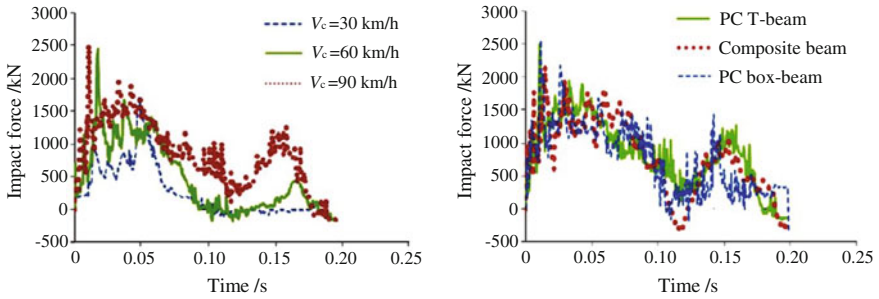

(a) By different truck velocities (b) For different bridge structural types

Fig. 8.14 Time histories of lateral impact forces by truck collision with bridge

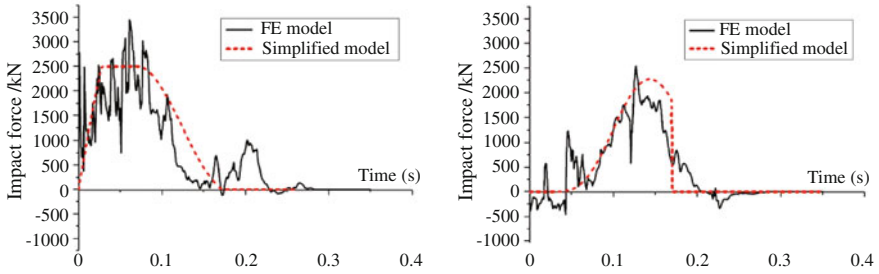

Fig. 8.15 Comparison of collision force histories by simplified model and FE method (V = 60 km/h)

quasi-static analysis to the dynamic analysis. The proposed procedure can be used for the design of RC columns to minimize damage and meet a set of performance objectives during different vehicle impact scenarios and can be extended to estimate the capacity of other members such as prestressed columns, steel columns, and beams and other hazards such as high-velocity impacts due to blasts or missiles. Shown in Fig. 8.16 are the failure modes of the column and two types of trucks after collision.

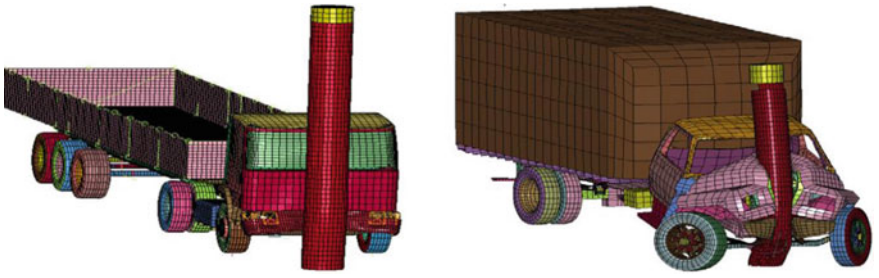

(a) 38-t truck, V_c = 18 m/s, no column failure. (b) 8-t truck, V_c = 32m/s, with column failure.

Fig. 8.16 FE simulation of an RC column collided by trucks

These research results show that in general, the time histories of impact force from vehicle collision with pier exhibit a characteristic of pulse waveform; the faster the vehicle velocity, the earlier the peak appears, and the narrower the pulse width, with very short loading duration usually less than 0.2 s. The heavier the vehicle, the faster the vehicle velocity, and the shorter the loading duration, the greater the instant collision force, with the maximum being dozens of MN.

8.1.3 Collision by Drifting-Floe

In addition to collisions by vessels and vehicles, the pier of a bridge crossing a river may be collided by drifting-floe or other floating objects. In particular, for the drifting-floe with large volume and huge impact energy, it may have a destructive impact on the structure; thus, the collision of ice-floe on bridge piers has been paid more attention by researchers.

There are two types of ice effects on structure: static ice load and dynamic ice load. The static ice load concerns the maximum static ice force on the structure, which is used to determine the static stiffness and strength of the structure, to ensure it against damage. The dynamic ice load concerns not only the maximum instant ice force, but also the variation of the force with time, which may induce the vibration of bridge. The dynamic ice load affects the structure response in its loading form, magnitude, and duration. Only by the characteristics of the dynamic ice load, can the structural response be exactly evaluated, so as to avoid structural damage caused by overlarge vibrations. However, the current bridge design codes only give the design formulas for static ice load, which are not applicable for dynamic analysis of bridges subjected to ice collision. With the occurrence of many ice-excited vibration accidents, this issue has been more and more noticed.

The dynamic ice load is complex, which is divided into three categories as periodic, random, and impact (Yu et al. 2009a, b; Guo 2010). Each category of dynamic ice load has its distinct feature in impact force magnitude, loading duration, and variation speed. In the three categories, the dynamic ice load caused by drifting-floe impact on a bridge pier is most concerned in train-bridge coupling dynamic analysis, so it is summarized as herein below.

There are two methods for studying ice-floe collision with pier, namely experiment, and numerical simulation.

The experimental study includes the in situ test and the laboratory test. The data measured at in situ test can well reflect the real ice-floe collision, but they are not easy to obtain, because under the difficult in situ test condition, the sensors always directly contact with the water and are often damaged by the impact of the huge ice-floe, and moreover, the free ice-floe drifting state cannot be controlled. The current studies are mainly concentrated on the fracture performance of ice-floes, while very few for direct measurement of their collision forces with bridge piers.

From the laboratory test, various factors affecting the ice-floe collision with piers can be accurately measured and quantitatively analyzed, by changing the

mechanical features, volumes, and drifting velocities of ice-floes and the structural parameters of the collided pier. However, due to the mechanical behavior of ice-floe that has a significant size effect, the scaled model test can hardly reflect the complicated conditions on the site.

With the development of numerical simulation techniques, the study on ice-structure collision based on various finite element models has achieved considerable progress. The ice loads, especially the dynamic ice loads, are rather complex, which depend not only on the mechanical characteristics of the ice and the type of the collided structure, but also on the dynamic interaction between the ice-floe and the structure. Because in-depth study of these issues is beyond the scope of this book, herein with the need of research in this chapter, several typical ice-collision loads obtained by experiments and finite element simulations are introduced.

Liu (2011) implemented the numerical simulations of interaction processes between sea ice and bridge foundation according to the condition of sea ice in Qingdao Gulf. The results showed that when the flow velocity is larger than 0.1 m/s, the ice crushing failure is formed, and during the crushing process it produces the dynamic force on the structure, as shown in Fig. 8.17a. In the case of the impact force curve, a strong impact pulse occurs very soon after the collision, with duration of about 0.5 s, and subsequently, with the process of impact, squeeze, and crushing the ice body suffered, there appears a series of smaller magnitude. This is in accordance with the model test result in Fig. 8.17b (Tuhkuri 1995).

Wu et al. (2008) conducted numerical simulations of bending failure processes between sea ice and conical structure, using the software LS-DYNA, and obtained the impact force time history of ice-floe, as shown in Fig. 8.17c. Zhang et al. (2002) analyzed the dynamic interaction between ice and structure by the DDA (discontinuous deformation analysis) approach, and with the inverse analysis on the structural response, a similar ice impact force acting on the structure is obtained, as shown in Fig. 8.17d.

Dong et al. (2012) conducted a series of tests of ice loads on cylindrical piles subjected to the impacts of drifting ice and obtained the ice impact force on the pier, as shown in Fig. 8.18a, which is similar to that from a field measurement by Guo (2010) shown in Fig. 8.18b. In these curves, the impact forces reach the peak within a very short time after the collision and then sharply decline, showing a typical pulse load. They then analyzed the relationship between ice kinetic energy and the impact force, finding that the design load on the piles can be determined with an envelope of logarithm curve.

Han (2000) conducted a field experiment on drifting-floe colliding with the No. 3 pier of the Harbin Songhua River Bridge. By installing five ice-pressure sensors on the ice guard, she measured the dynamic pressures of the floating floe on the pier and observed the crushing state of the floe when it collided with the guard body. Shown in Fig. 8.19 are two typical measured dynamic pressure signals under ice-floe collision, from which the maximum impact force was acquired, by scaling with the calibrated rate, as 507.6 kN.

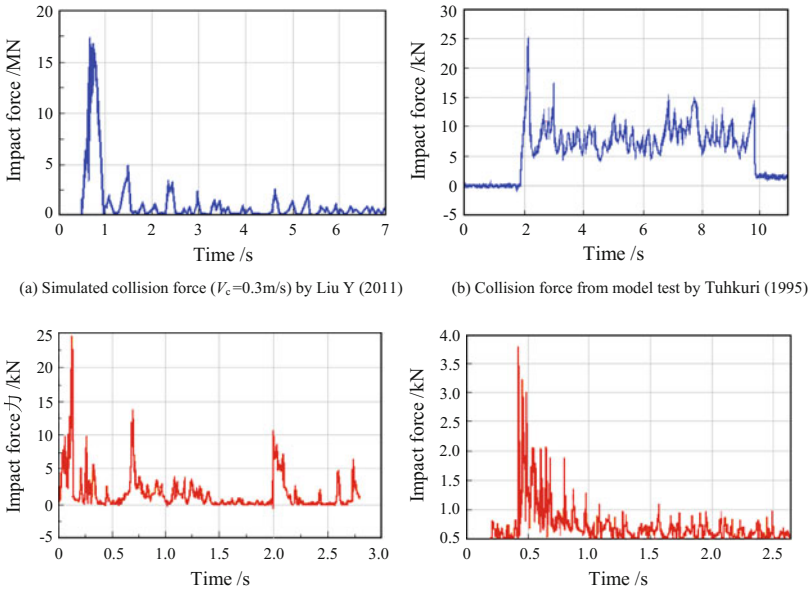

(a) Simulated collision force (V_c=0.3m/s) by Liu Y (2011)

(b) Collision force from model test by Tuhkuri (1995)

(c) Simulated collision force (V_c=1.0m/s) by Wu WH (2008)

(d) Simulated collision force (V_c=1.0m/s) by Zhang YL *et al*. (2002)

Fig. 8.17 Impact force time histories of ice-floe collision with structures

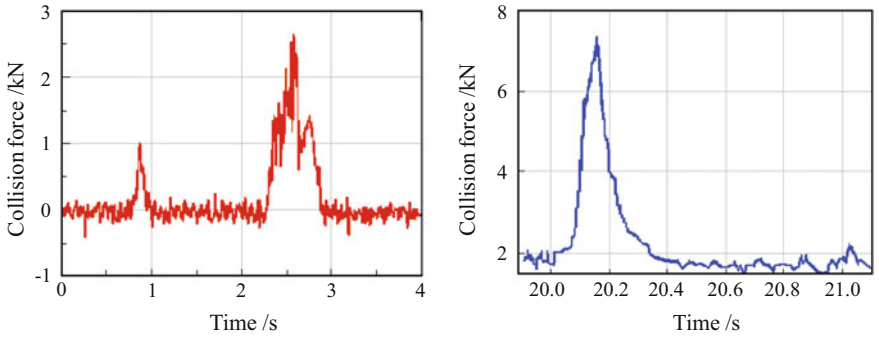

(a) Model test by Dong JW *et al*. (2012).

(b) Field experiment by Guo FW (2010).

Fig. 8.18 Impact force time histories of ice-floe collision by model test and field measurement

In the springs of 2008 ~ 2010, the author participated in the field experiments at several bridges suffering drifting-floe collision in the cold Northeast China (Yu et al. 2009; Xia et al. 2012a, b), measured the impact forces of the floes colliding with the piers, and recorded the statuses of the collisions. Shown in Fig. 8.20 are

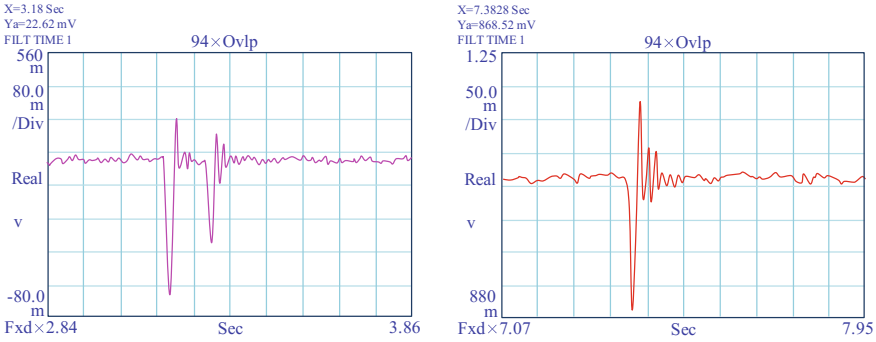

Fig. 8.19 Dynamic pressure signals under ice-floe collision measured at No. 3 pier of the Harbin Songhua River Bridge

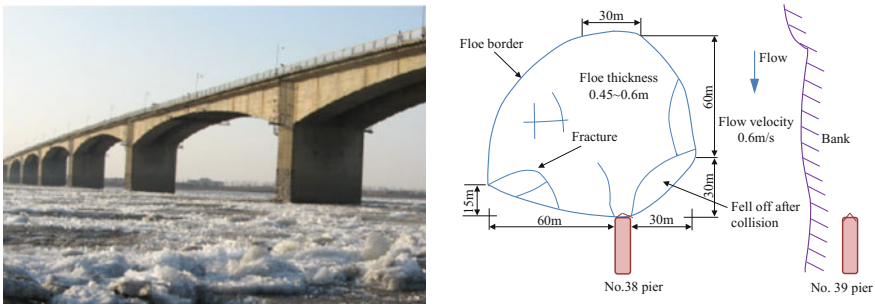

Fig. 8.20 Ice-floes drifting on the Tonghe Songhua River and a 90 m × 90 m floe colliding with the No. 38 pier of the bridge (maximum impact force 315.83 kN)

the scene of ice-floes drifting on the Tonghe Songhua River and the status of a 90 m × 90 m huge floe colliding the No. 38 pier of the bridge.

Summarized in Table 8.1 are maximum impact forces of ice-floe collision with piers measured at several bridges, with the respective geometries and flowing velocities of the floes.

In these experimental results, the maximum impact force of ice-floe collision was 2432.82 kN, measured at the No. 10 pier of the Jiamusi Songhua River Bridge, the area of the ice-floe was recorded as 80 × 60 m^2, and the flow velocity 1.35 ~ 1.45 m/s. Shown in Fig. 8.21a is the impact force time history of this collision. The impact load exhibits a typical repeated-impact feature, with the duration of about 4 s; the maximum force appeared at about 0.26 s and subsequently followed three peaks around 850 kN and one around 500 kN between 0.5 ~ 2.5 s; and afterward, at the end of this collision, appeared the second biggest peak of 1500 kN at about 3.7 s.

Table 8.1 Results of ice-floe collision with piers measured at bridge sites

No.	Bridge name	Pier No.	Floe size (m^2)	Floe velocity (m/s)	Max. impact force (kN)
1	Huma River Bridge	No. 1	60 × 80	0.85	1968.82
2	Xunbila River Bridge	No. 7	20 × 20	——	280
3	Jiamusi Songhua River Bridge	No. 10	80 × 60	1.35 ~ 1.45	2432.82
4	Tonghe Songhua River Bridge	No. 38	80 × 100	0.45 ~ 0.60	375.48
5	Harbin Songhua River Bridge	No. 3	60 × 100	——	387.1

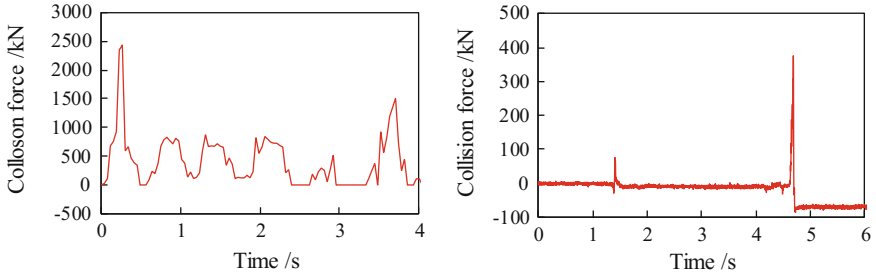

(a) No. 10 pier of Jiamusi Songhua River Bridge (b) No. 38 pier of Tonghe Songhua River Bridge

Fig. 8.21 Impact force time histories of ice-floe collision with piers measured at bridge sites

Shown in Fig. 8.21b is another typical impact force time history of ice-floe collision, which was measured at the No. 38 pier of the Tonghe Songhua River Bridge, the area of the ice-floe was recorded as 80 × 100 m^2, the thickness was 0.45 ~ 0.60 m, and the flow velocity was 0.6 m/s. There appeared two pulses in the impact force time history: The first small pulse was 75.34 kN with a short duration of about 0.02 s, and 3.3 s after it, the second pulse appeared, with a bigger peak of 375.48 kN and a longer duration of 0.16 s.

To study the collision intensity of ice-floe, Timco et al. (2003, 2011) summarized all available data related to ice-floe impacts on structures, including laboratory tests, forces on several bridge piers (Hondo, Pembina, Rideau), forces from small icebergs impacting dedicated test structures (Grappling Island, Newmans Cove), multi-year ice impacts on the offshore structure Molikpaq, and the Hans Island experiments. Based on statistical analysis, they found the impact force was best related to the kinetic energy of the floe at impact. This energy ranged over thirteen orders of magnitude in value, showing a good correlation of the impact force F with the energy E at impact with a function form $F = Ae^{0.532}$ where the coefficient A was determined to be 61.7 MN for the "likely" impact force and 388 MN for the

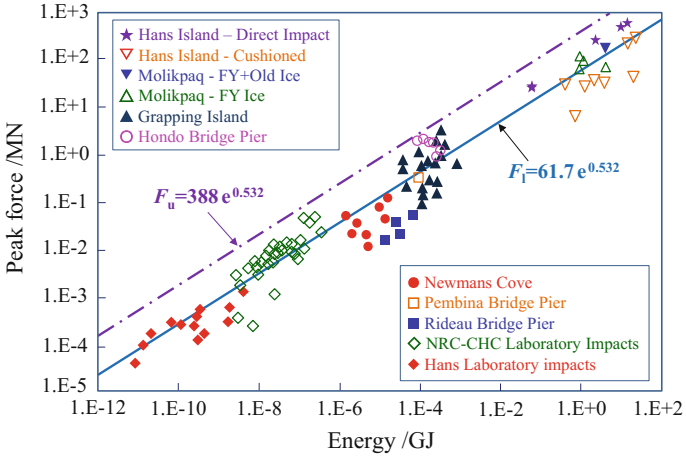

Fig. 8.22 Distribution of peak impact force versus the kinetic energy of ice-floe

upper-limit, as shown in Fig. 8.22. The figure shows that the maximum impact force of ice-floe can be hundreds of MN.

These research results show that in general, the time histories of ice-floe collision forces exhibit a characteristic of pulse waveform; the faster the flow velocity, the greater the instant force, and the shorter the impact action, being 0.05 $\sim$ 0.5 s, with wide duration range of 0.05 $\sim$ 4.0 s; the heavier the ice-floe, and the faster the flow velocity, the greater the instant collision force, with the maximum being hundreds of MN.

8.1.4 Characteristics of Bridge Collision Loads

The collision loads on bridge structure concerned in train-bridge coupling dynamic analysis mainly include vessel collision, vehicle collision, and ice-floe collision. These collision loads are very complicated, with their respective characteristics in impact force time histories, maximum impact forces, and acting positions, as summarized in Table 8.2.

Table 8.2 Characteristics of various bridge collision loads

Collision loads	Vessel collision	Vehicle collision	Drifting-floe collision
Impact force time history	Time history of impact force exhibits a characteristic of strong nonlinear waveform, with loading durations of 3 ~ 4 s	Time history of impact force exhibits a characteristic of pulse waveform. The faster the vehicle velocity, the earlier the peak appears, and the narrower the pulse width, with very short loading duration of usually less than 0.2 s	Time history of impact force exhibits a characteristic of pulse waveform. The faster the flow velocity, the greater the instant force, and the shorter the impact action, being 0.05 ~ 0.5 s, with wide duration range of 0.05 ~ 4.0 s
Maximum Impact force	The heavier the vessel, and the faster the impact velocity, the greater the instant collision force, with the maximum hundreds of MN	The heavier the vehicle, the faster the vehicle velocity, and the shorter the loading duration, the greater the instant collision force, with the maximum dozens of MN	The heavier the floe, and the faster the flow velocity, the greater the instant collision force, with the maximum hundreds of MN
Position of impact	Acting on pier at position varying with the navigation water level and colliding part of the vessel; sometimes on superstructure	Acting on pier usually at low position; sometimes on superstructure	Acting on pier at the flow surface, varying with the water level

8.2 Dynamic Analysis Model of Train-Bridge System Subjected to Collision Loads

When a bridge is collided by a vessel, a car or other colliding object, the analysis model of the train-bridge system can be regarded as a spatial dynamic system composed of three subsystems: the bridge subsystem, the train subsystem, and the colliding object subsystem, as shown in Fig. 8.23.

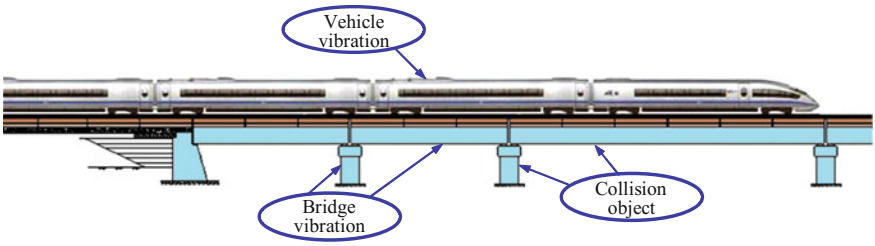

Fig. 8.23 A coupled train-bridge system subjected to a vessel collision

Theoretically, the motion equations for such a system can be expressed as

$$\begin{bmatrix} \mathbf{M}_{vv} & 0 & 0 \\ 0 & \mathbf{M}_{bb} & 0 \\ 0 & 0 & \mathbf{M}_{cc} \end{bmatrix} \begin{Bmatrix} \ddot{\mathbf{X}}_v \\ \ddot{\mathbf{X}}_b \\ \ddot{\mathbf{X}}_c \end{Bmatrix} + \begin{bmatrix} \mathbf{C}_{vv} & \mathbf{C}_{vb} & 0 \\ \mathbf{C}_{bv} & \mathbf{C}_{bb} & \mathbf{C}_{bc} \\ 0 & \mathbf{C}_{cb} & \mathbf{C}_{cc} \end{bmatrix} \begin{Bmatrix} \dot{\mathbf{X}}_v \\ \dot{\mathbf{X}}_b \\ \dot{\mathbf{X}}_c \end{Bmatrix} + \begin{bmatrix} \mathbf{K}_{vv} & \mathbf{K}_{vb} & 0 \\ \mathbf{K}_{bv} & \mathbf{K}_{bb} & \mathbf{K}_{bc} \\ 0 & \mathbf{K}_{cb} & \mathbf{K}_{cc} \end{bmatrix} \begin{Bmatrix} \mathbf{X}_v \\ \mathbf{X}_b \\ \mathbf{X}_c \end{Bmatrix} = \begin{Bmatrix} \mathbf{F}_{vb} \\ \mathbf{F}_{bv} + \mathbf{F}_{bc} \\ \mathbf{F}_{cb} \end{Bmatrix} \tag{8.11}$$

where the subscripts "v", "b", and "c" represent the train, bridge, and colliding objects, respectively; **M**, **C,** and **K** are the mass, damping, and stiffness matrices of the train-bridge system, respectively; **X**, $\dot{\mathbf{X}}$, and $\ddot{\mathbf{X}}$ are the displacement, velocity, and acceleration vectors, respectively; $\mathbf{F}_{vb}$ and $\mathbf{F}_{bv}$ are the interforce vectors of the bridge to the train and the train to the bridge; and $\mathbf{F}_{bc}$ and $\mathbf{F}_{cb}$ are the interforce vectors of the colliding object to the bridge and the bridge to the colliding object, respectively.

It should be noticed that the colliding object may produce plastic deformation during the collision, and the bridge may be damaged if the collision load is sufficiently large. In this case, the structural characteristics of the colliding object and the bridge may be changed, so the influence of nonlinear factors on the stiffness matrices $\mathbf{K}_{bb}$, $\mathbf{K}_{bc}$, $\mathbf{K}_{cb}$, and $\mathbf{K}_{cc}$ related to the colliding object and the bridge in Eq. (8.11) should be considered.

However, the coupling vibration of train-bridge system under collision loads is a complex problem. The complexity contains the following: (1) the characteristics of the collision load, whatever it is induced by vessel, vehicle, ice-floe, or other colliding objects, not only relate to the mass and motion speed of the colliding object, but also depend on the stiffness of the colliding object and the collided structure; (2) the stiffness of the colliding object that is related to its own material and structural characteristics, such as the material and the structure of the vessel bow and the anti-collision beam of the vehicle, and the hardness and shape of the ice-floe. The colliding object and the collided object with different stiffness have different deformation and energy absorption capacities, which directly influence the time histories of the collision load, such as the duration time and collision strength. Therefore, synchronously considering the interactions between train and bridge and between colliding object and collided structure makes the problem extremely complicated, which is almost unrealizable by the current analysis methods.

On the other hand, according to the existing researches, there are three methods to obtain the collision load: field test, model experiment, and numerical simulation. Whatever any method is used, the time history of the acquired collision load has included the influence of the stiffness and the deformation of the colliding object and the collided structure, and also the dynamic interaction between them. Therefore, with a known collision load, it is feasible to use a simplified method to analyze the dynamic responses of train-bridge system under collision load: By neglecting the interaction between the colliding object and the bridge structure, the time history of the collision load is directly taken as the input excitation on the train-bridge system, to solve the problem through simulation analysis.

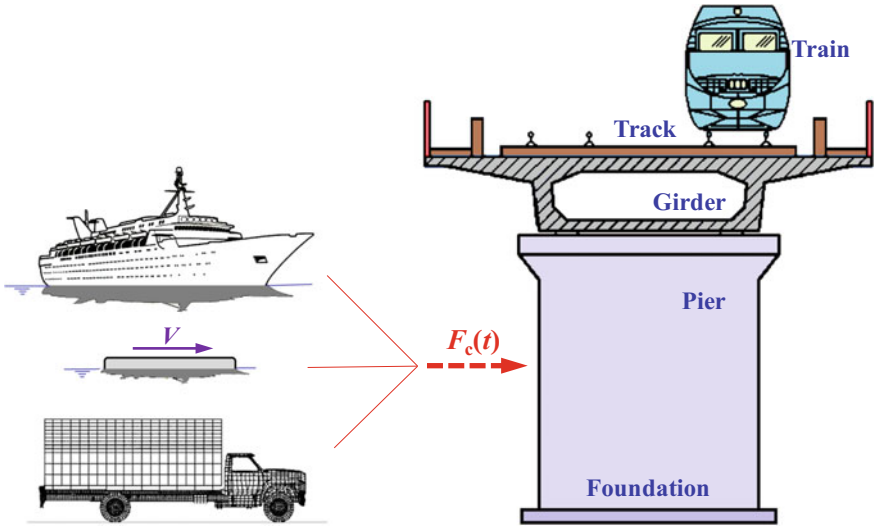

Fig. 8.24 Dynamic model for train-bridge system subjected to collision loads

The train-bridge dynamic interaction model established by this method is shown in Fig. 8.24, which consists of two subsystems, the train subsystem and the bridge subsystem, and the collision load is directly applied on the bridge structure as the external force $F_c(t)$.

In the analysis, the train subsystem model is established by rigid bodies with elastic connections, and the bridge subsystem model is established either by the FEM (Finite element method) or the MDM (modal decomposition method). The two subsystems are coupled by the wheel-rail interaction, and the track irregularity is regarded as the internal excitation of the two subsystems.

When the bridge subsystem is established by the FEM, the coupled motion equations for the train-bridge system subjected to collision loads can be expressed as

$$\begin{bmatrix} \mathbf{M}_{vv} & 0 \\ 0 & \mathbf{M}_{bb} \end{bmatrix} \begin{Bmatrix} \ddot{\mathbf{X}}_v \\ \ddot{\mathbf{X}}_b \end{Bmatrix} + \begin{bmatrix} \mathbf{C}_{vv} & \mathbf{C}_{vb} \\ \mathbf{C}_{bv} & \mathbf{C}_{bb} \end{bmatrix} \begin{Bmatrix} \dot{\mathbf{X}}_v \\ \dot{\mathbf{X}}_b \end{Bmatrix} + \begin{bmatrix} \mathbf{K}_{vv} & \mathbf{K}_{vb} \\ \mathbf{K}_{bv} & \mathbf{K}_{bb} \end{bmatrix} \begin{Bmatrix} \mathbf{X}_v \\ \mathbf{X}_b \end{Bmatrix} = \begin{Bmatrix} \mathbf{F}_{vb} \\ \mathbf{F}_{bv} \end{Bmatrix} + \begin{Bmatrix} 0 \\ \mathbf{F}_c \end{Bmatrix} \tag{8.12}$$

where the subscripts "v" and "b" represent the train and the bridge, respectively; **M**, **C**, and **K** are the mass, damping, and stiffness matrices, and **X**, $\dot{\mathbf{X}}$, and $\ddot{\mathbf{X}}$ are the displacement, velocity, and acceleration vectors, respectively; $\mathbf{F}_{vb}$ and $\mathbf{F}_{bv}$ are the interforce vectors of the bridge structure and the train vehicles, respectively. Details of these matrices and vectors can be found in Chap. 5 of this book.

When the bridge subsystem model is established by the MDM, the motion equation of the system can be expressed as

$$\begin{bmatrix} \mathbf{M}_{vv} & 0 \\ 0 & \mathbf{M}_{bb} \end{bmatrix} \begin{Bmatrix} \ddot{\mathbf{X}}_v \\ \ddot{\mathbf{Q}}_b \end{Bmatrix} + \begin{bmatrix} \mathbf{C}_{vv} & \mathbf{C}_{vb} \\ \mathbf{C}_{bv} & \mathbf{C}_{bb} \end{bmatrix} \begin{Bmatrix} \dot{\mathbf{X}}_v \\ \dot{\mathbf{Q}}_b \end{Bmatrix} + \begin{bmatrix} \mathbf{K}_{vv} & \mathbf{K}_{vb} \\ \mathbf{K}_{bv} & \mathbf{K}_{bb} \end{bmatrix} \begin{Bmatrix} \mathbf{X}_v \\ \mathbf{Q}_b \end{Bmatrix} = \begin{Bmatrix} \tilde{\mathbf{F}}_{vb} \\ \tilde{\mathbf{F}}_{bv} \end{Bmatrix} + \begin{Bmatrix} 0 \\ \tilde{\mathbf{F}}_c \end{Bmatrix} \tag{8.13}$$

where $\mathbf{Q}_b$, $\dot{\mathbf{Q}}_b$, and $\ddot{\mathbf{Q}}_b$ are the modal displacement, velocity, and acceleration vectors of the bridge subsystem, respectively; $\tilde{\mathbf{F}}_{vb}$ and $\tilde{\mathbf{F}}_{bv}$ are the interforce vectors of the train vehicle and the bridge subsystem with modal coordinates. The modal displacement $\mathbf{Q}_b$ can be acquired using the following transform formula:

$$\mathbf{Q}_b = [\, q_1 \quad q_2 \quad \cdots \quad q_n \quad \cdots \quad q_{N_b} \,] = \mathbf{\Phi}^T \mathbf{X}_b \tag{8.14a}$$

$$q_n = \sum_{k=1}^{N} \phi_n(k) X(k) \tag{8.14b}$$

where q_n is the nth modal coordinate of the bridge; $\mathbf{\Phi}$ is the mode-shape matrix of the bridge; $\phi_n(k)$ is the value of the nth modal function of the bridge at the kth node; N_b is the total number of the bridge modes concerned; $X(k)$ is the bridge displacement at the kth node; and N is the total number of bridge nodes.

According to the related design codes in China, for the bridge pier and abutment located in a navigable river or a river with floating objects, the collision by vessel or floating object should be considered in the design. For the bridge across a railway or highway, the collision on the pier and abutment by the vehicle should also be considered. In a general design, the collision load can be calculated by the related equations in the codes. In the present bridge code, however, the calculation method for the collision load is still at the static design stage, which cannot be used directly for calculating the dynamic response of the train-bridge system subjected to a collision load. Instead, the time history of the collision load is needed, which is input to the train-bridge system as an external excitation to carry out the simulation calculation.

When the bridge model is established by the FEM, the collision load on the bridge can be applied to the related structural nodes as the collision load vector $\mathbf{F}_c$. When the bridge model is established by the MDM, the generalized collision load vector $\tilde{\mathbf{F}}_c$ corresponding to the related modes can be expressed as

$$\tilde{\mathbf{F}}_c = \mathbf{\Phi}^T \mathbf{F}_c = [f_{c1}(t), f_{c2}(t), \cdots f_{cn}(t), \cdots f_{cN_b}(t)]^T \tag{8.15}$$

where f_{cn} is the generalized collision force acting on the bridge corresponding to the nth mode. Supposing the collision forces act horizontally on the pier, f_{cn} can be expressed as

$$f_{cn} = \sum_{k=1}^{N} \phi_n^{\mathrm{h}}(k) F_k(t) \tag{8.16}$$

where $\phi_n^{\mathrm{h}}(k)$ is the function value of the nth mode shape in horizontal direction of the bridge at the kth node; $F_k(t)$ is the collision force history of the vessel on the bridge at the kth node, which is only different from zero at the pier nodes affected by the collision.

When the collision load is known as an external load, the motion equations for the train-bridge interaction system subjected to a collision load can be solved by the software for dynamic analysis of train-bridge interaction system.

8.3 Dynamic Analysis of Train-Bridge System Subjected to Collision Loads

Using the established model, the whole process of a train passing through the bridge subjected to collision loads can be simulated, to calculate the dynamic responses of the bridge and the running safety indices of the on-bridge train, and further to analyze the characteristics of time histories and frequency spectra.

8.3.1 Bridge Description and Calculation Parameters

The case study concerns a double-track bridge situated on the Harbin-Dalian HSR line in Northeast China. The bridge is composed of (32+48+32) m continuous PC box-girders, with two 32 m simply-supported side spans added at both ends of the continuous span, as shown in Fig. 8.25.

The cross section and the main dimensions of the girder are shown in Figs. 8.26 and 8.27. The widths of top slab and bottom plate are 13.4 m and 5.74 m, respectively, and the depth of the girder is 3.0 m for the whole span length, while at the strengthened segments of 500 cm long (250 cm each side from the bearing

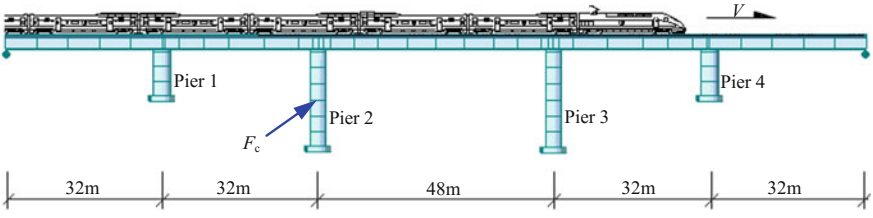

Fig. 8.25 Configuration of the (32 + 48 + 32) m continuous bridge with two 32 m side spans

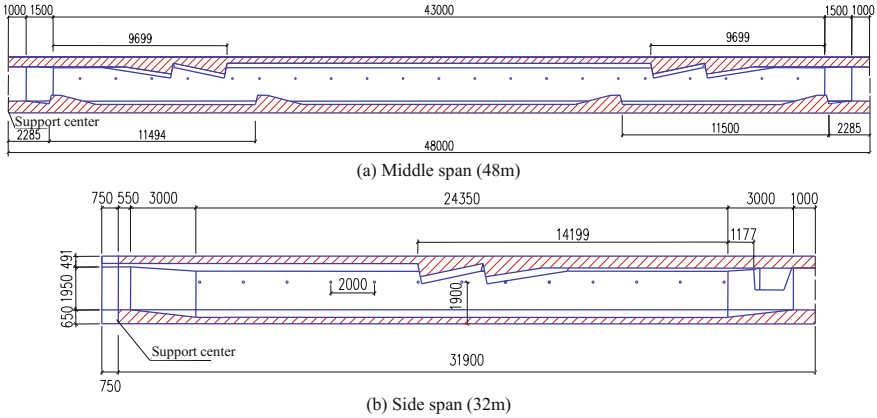

Fig. 8.26 Elevations of the (32+48+32) m continuous bridge (unit: mm)

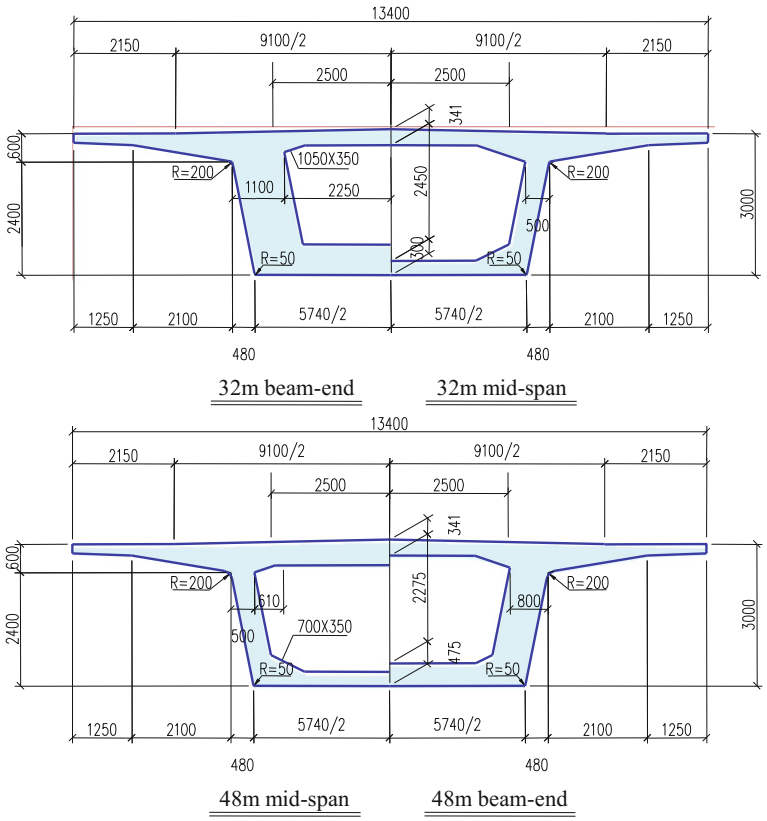

Fig. 8.27 Cross sections of the (32+48+32) m continuous bridge (unit: mm)

Table 8.3 Foundation stiffness of the (32+48+32) m continuous bridge piers

Pier		Section area (m^2)	Translational stiffness (MN/m)		Rotational stiffness (MN·m/rad)		
			R_x	R_y	R_z	M_x	M_y
Middle piers	Fixed bearing	7.75 × 4.45	1681.59	1681.59	13328.5	189480	189480
	Movable bearing	7.75 × 4.45	1683.91	1683.91	13906.7	197110	197110
Side piers		7.0 × 3.2	892.11	882.91	7725.1	83424	45567
Middle piers	Fixed bearing	7.75 × 4.45	13328.5	1681.59	189480	1681.59	189480
	Movable bearing	7.75 × 4.45	13906.7	1683.91	197110	1683.91	197110
Side piers		7.0 × 3.2	7725.1	892.11	45567	882.91	83424

center) above the Piers 2 and 3, the upper slab, bottom plate, and the webs are thickened. Laid on the bridge deck are the CRTS II ballastless double slab tracks, and the secondary phase dead load applied on the bridge model is 18.5 t/m.

The substructure of the bridge includes the concrete solid piers with round-ended sections and the concrete pile foundations. The height of two middle piers is 19.45 m, and the height of two side piers is 10.0 m. In the finite element model, the piers are modeled with beam elements and the support stiffness of pile foundations is considered, as listed in Table 8.3, in which R_x, R_y, and R_z are translational stiffness in longitudinal, transverse, and vertical directions, and M_x and M_y are rotational stiffness around the longitudinal and transverse axes of the bridge, respectively, provided by the designer.

For the (32+48+32) m continuous spans, mounted on the Pier 2 are fixed pot neoprene bearings, while the rest are sliding ones. In the analysis, the bearings are modeled according to the design. For the sliding bearing, the translational displacement in the longitudinal x-axis and the rotational angle about transverse y-axis of the girder end are free, while the other 2 translational displacements and 2 rotational angles are modeled as slave DOFs of the master DOFs at the pier-top. For the fixed bearing, the rotational angle about the transverse y-axis of the girder end is free, while the other 3 translational displacements and 2 rotational angles are connected through master-and-slave relation to the pier-top.

By a finite element modal analysis, the natural vibration characteristics including frequencies and mode shapes of the bridge are obtained. Shown in Table 8.4 are the first 10 modes with their characteristics in frequencies and mode shapes.

The high-speed train ICE3, which was used in China for the dynamic analysis of high-speed railway bridges, is adopted. The train is composed of (3 M + 1T) × 3 cars, with M representing the motor-car and T the trailer-car, respectively. The average axle loads are 156.96 kN for the motor-car and 143.23 kN for the trailer-car. Other parameters can be found in Table 6.8. Illustrated in Fig. 8.28 are the axle loads of a unit of ICE3 train with the main axle interval parameters.

Table 8.4 Dynamic properties of the (32+48+32) m continuous bridge on high-speed railway

Order of mode	Frequency (Hz)	Descriptions of vibration modes
1	3.351	Vertical symmetric bending
2	4.122	Lateral symmetric bending
3	4.994	Longitudinal bending with antisymmetric vertical bending
4	5.714	Longitudinal bending with antisymmetric vertical bending
5	6.347	Longitudinal bending with symmetric vertical bending
6	6.711	Lateral antisymmetric bending
7	7.785	Vertical antisymmetric bending
8	8.426	Vertical symmetric bending
9	9.231	Lateral symmetric bending
10	10.688	Vertical antisymmetric bending

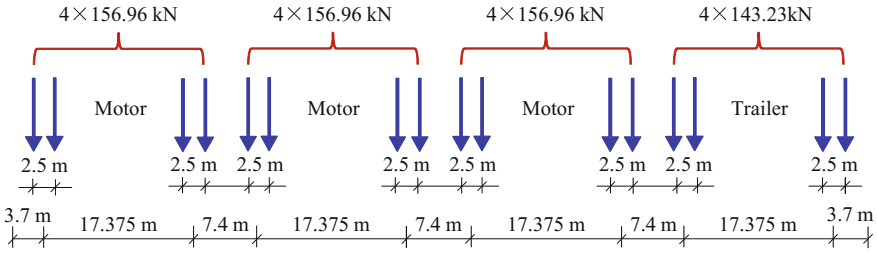

Fig. 8.28 Axle intervals and axle loads of a unit of ICE3 train

Three representative time histories and their spectra of collision loads are considered corresponding to ice-I load, ice-II load, and vessel load, as shown in Fig. 8.29.

It can be found that the time histories of collision loads are complicated during the collision with the piers:

For the ice-I load, it refers to the ice-floe collision load measured in the experiment on the Jiamusi Songhua River Bridge site in April 2009 (Xia et al. 2012a, b). It consists of six pulses acting repeatedly with an average width of 0.5 s and a total duration of 4 s.

The ice-II load was the ice-floe collision load measured in the experiment on the Tonghe Songhua River Bridge site in April 2010 (Xia et al. 2012a, b). It corresponds to a single pulse with a narrow pulse width of 0.06 s.

The vessel load is taken from the reference (Chen 2006) and represents the collision history by a ship, which is a wide continuous pulse with the total duration of 1.8 s.

In the analysis, the collision intensities (herein representing the maximum forces) of the three loads are normalized as 10 MN to compare the influence of different load histories, as shown in Fig. 8.29. As the three collision loads have different time evolutions, the dynamic responses of the bridge and the train will be different.

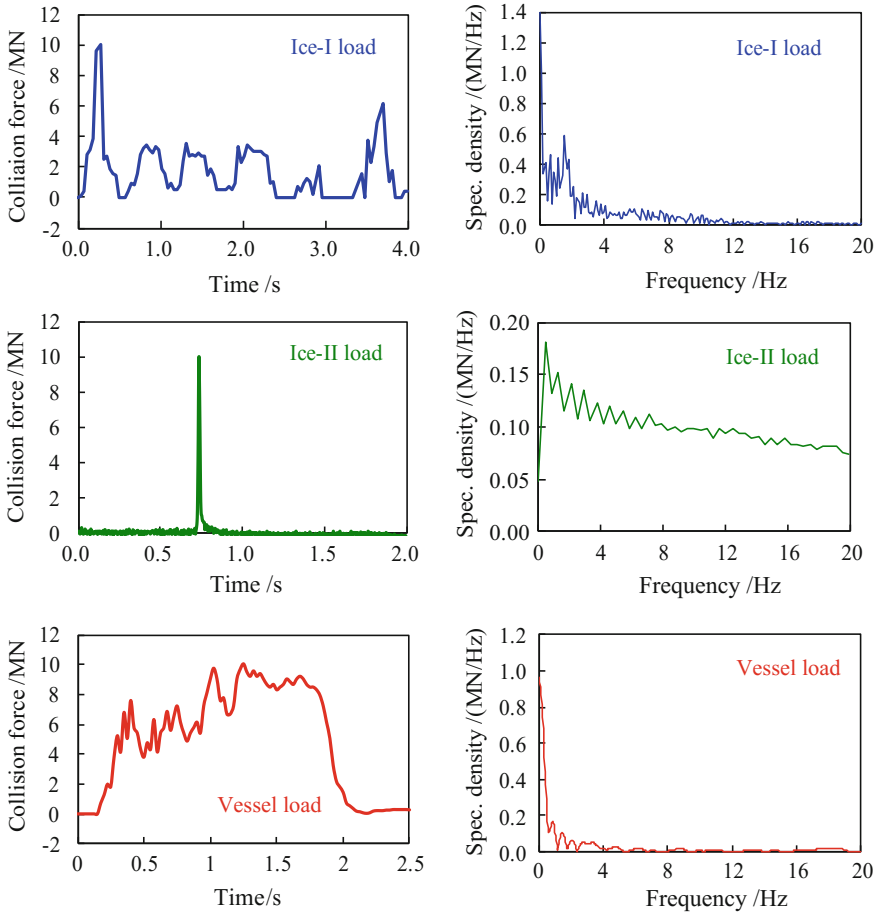

Fig. 8.29 Time histories and frequency spectra of collision loads

The three collision loads, in spite with identical intensity, have distinct features in impact velocity and duration, so they apply different effects on the dynamic responses of the bridge and the train vehicles, which will be analyzed hereinbelow.

The ICE3 train travelling on the bridge is simulated with and without collision. In the case with collision, the time history of the load is applied at level 10.2 m above the pile cap of the Pier 2, in the horizontal flow direction, as shown in Fig. 8.25. To better compare the results for different train speeds and different collision cases, each load is applied at the time when the train arrives at Pier 1, which ensures that some of the 12 cars of the train run on the first two continuous spans during the acting period of the collision load, in order to get the maximum vehicle responses.

The vertical, lateral, and rotational track irregularities are taken into consideration by using the data measured on the Qin-Shen HSR in China, as shown in Chap. 3. The damping ratio of bridge is 0.02, and the integration time step is 0.0005 s.

8.3.2 *Dynamic Responses of the Bridge*

Shown in Figs. 8.30 and 8.31 are the lateral displacement histories at the top of Pier 2 and at the mid-span (48 m middle span S4) of the bridge without collision and under three collision loads, when the ICE3 train travels on the bridge at the speed of V = 200 km/h.

From the figures, the effect of the collision is obvious:

(1) In the case without collision, the lateral displacements of the bridge are induced by the running train; therefore, the time history curves are steady with very small amplitudes, 0.063 mm for the pier-top and 0.066 mm for the mid-span. While under the collisions of ice-I load, ice-II load, and vessel load, the displacements are significantly amplified. The maximum displacements are 1.43 mm, 0.373 mm, and 1.24 mm for the pier-top, and 1.31 mm, 0.419 mm, and 1.09 mm for the mid-span, respectively.

(2) Loading rate and time duration of the collision loads have an obvious influence on the bridge displacements. For the ice-II load with the shortest pulse (0.06 s, much shorter than the first lateral period of the bridge), the most obvious impact effect in the displacement histories is induced, but the maximum peak value is relatively small. While for the ice-I and vessel loads with longer pulse widths (4 s and 1.8 s, respectively, both longer than the first lateral period of the bridge), the displacements at pier-top and mid-span are more than two times bigger than the ones induced by the ice-II load. This indicates that the load with longer duration time has a higher collision effect on the bridge displacement.

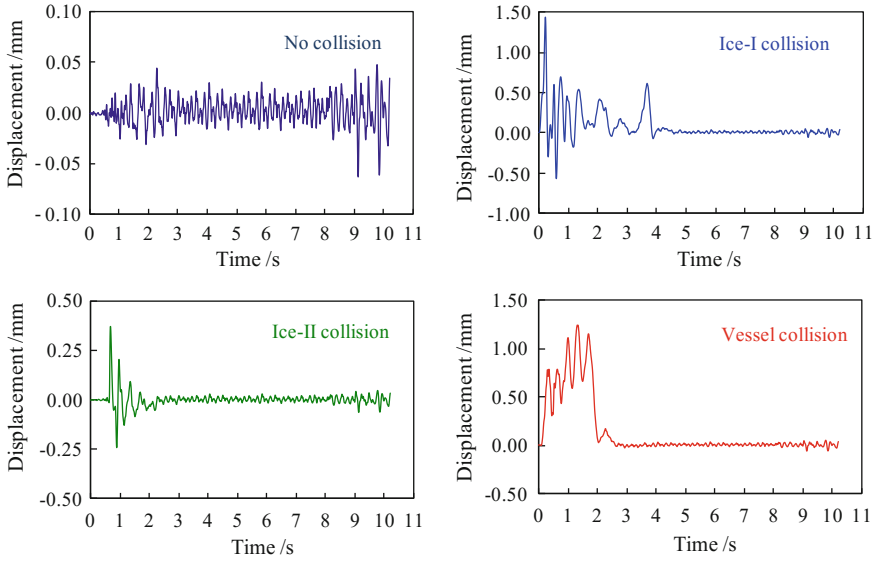

Fig. 8.30 Lateral displacements at the top of Pier 2 under V = 200 km/h

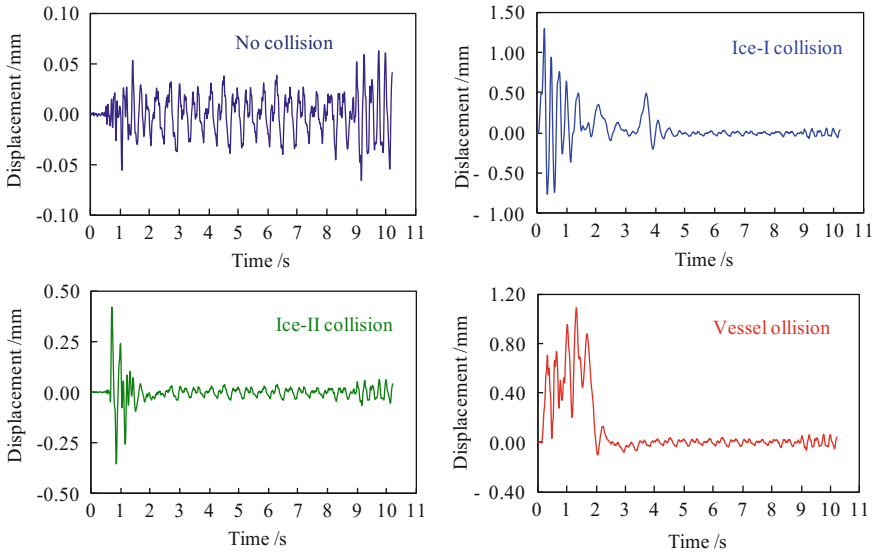

Fig. 8.31 Lateral mid-span displacements of the 48 m span under V = 200 km/h

(3) In the case with collision loads, the lateral displacement curves at the pier-top and mid-span of the bridge show clear impact characteristics. Owing to the damping action of the concrete pier and the girder, the vibrations attenuate fast, and the displacement curves return very soon to their steady state similar to the case without collision.

Shown in Figs. 8.32 and 8.33 are, respectively, the lateral acceleration histories at the top of Pier 2 and the mid-span (48 m middle span) of the bridge without collision and under the three collision loads, when the ICE3 train passes on the bridge at V = 200 km/h.

It can be observed from Figs. 8.32 and 8.33 that:

(1) In the case without collision, the time histories of the lateral accelerations are rather steady, with very small amplitudes of 23.0 cm/s^2 for the pier-top and 20.3 cm/s^2 for the mid-span. While under the collisions of ice-I load, ice-II load, and vessel load, the accelerations are greatly amplified, with the maximum values of 127 cm/s^2, 162 cm/s^2, and 73.5 cm/s^2 for the pier-top, and 135 cm/s^2, 100 cm/s^2, and 85.2 cm/s^2 for the mid-span, respectively.
(2) Owing to the damping action of the concrete pier and the girder, the accelerations attenuate fast, and the acceleration curves return very soon to their steady state similar to the case without collision.

The frequency contents of the bridge responses are shown in Figs. 8.34, 8.35, 8.36, and 8.37.

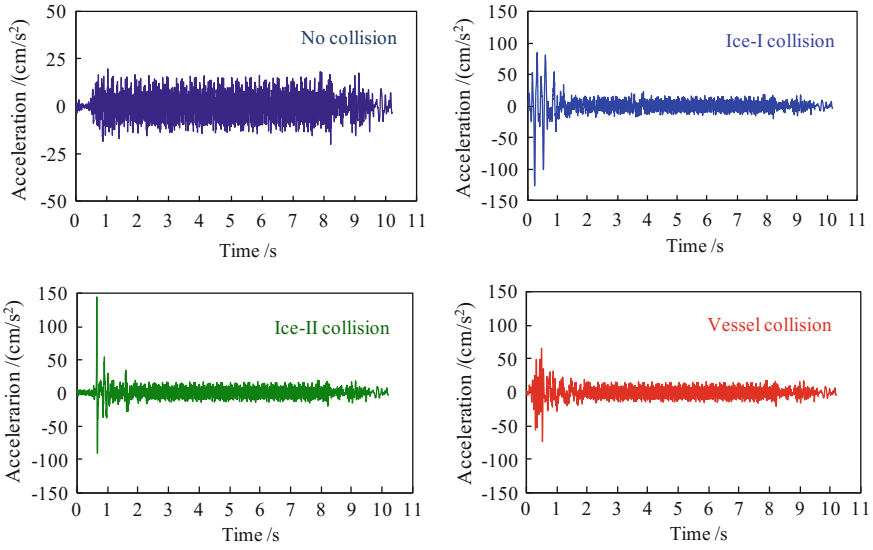

Fig. 8.32 Lateral accelerations at the top of Pier 2 under V = 200 km/h

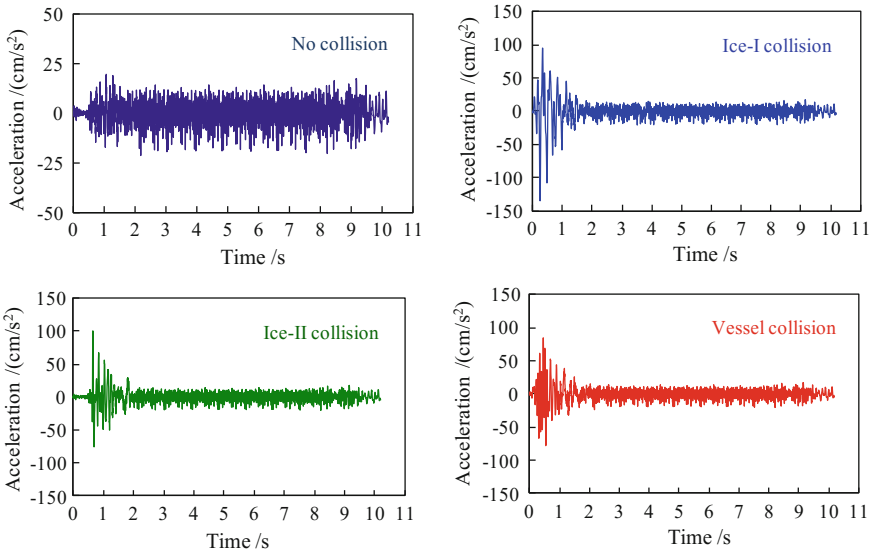

Fig. 8.33 Lateral mid-span accelerations of the 48 m span under V = 200 km/h

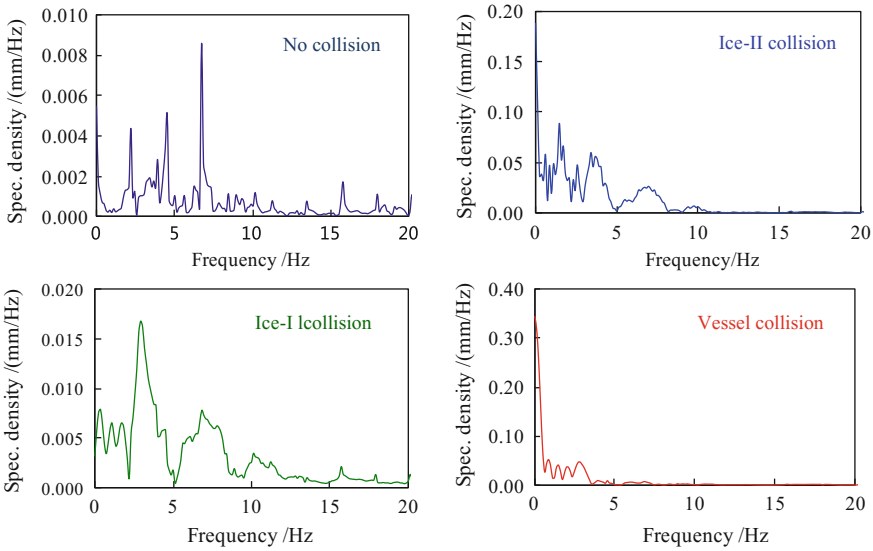

Fig. 8.34 Lateral displacement spectra at the top of Pier 2 under V = 200 km/h

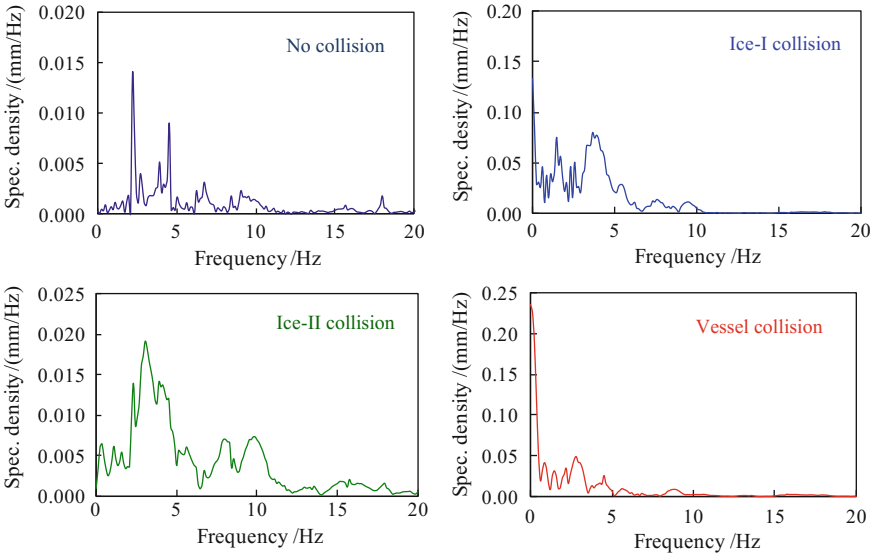

Fig. 8.35 Lateral displacement spectra of the 48 m mid-span under V = 200 km/h

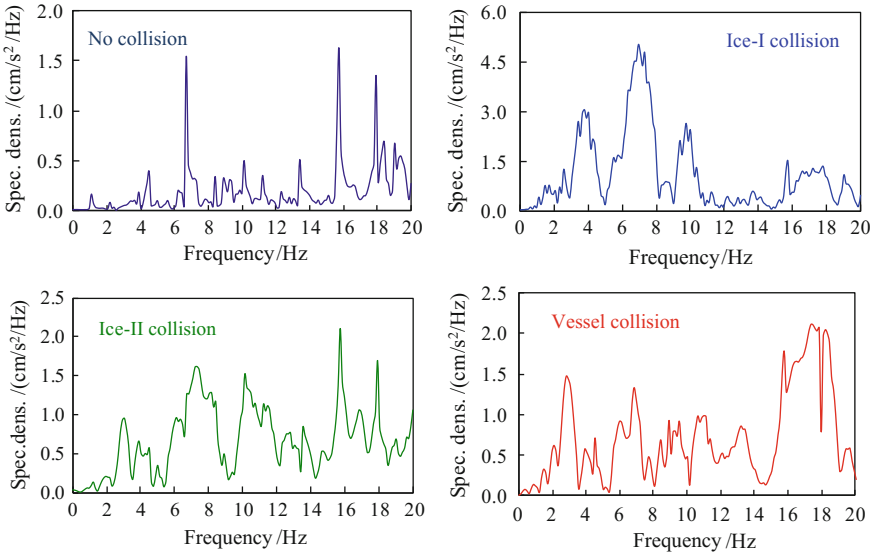

Fig. 8.36 Lateral acceleration spectra at the top of Pier 2 under V = 200 km/h

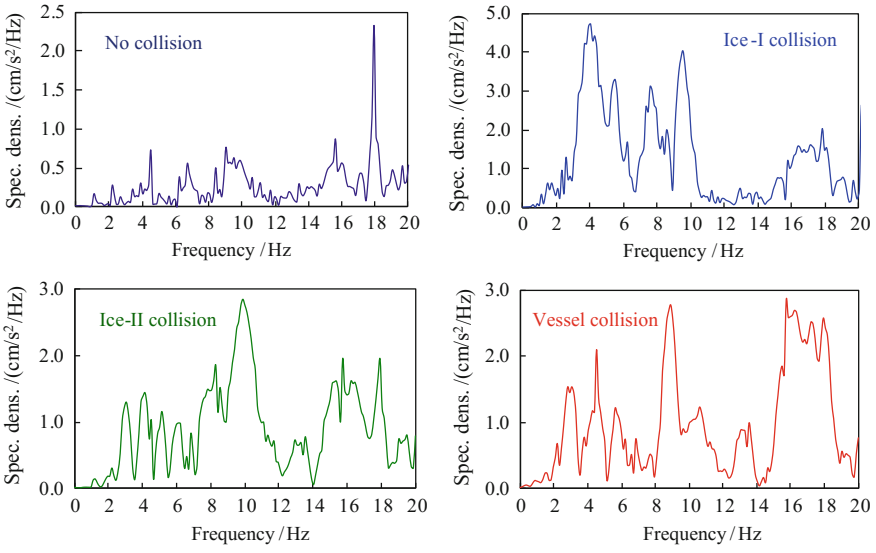

Fig. 8.37 Lateral acceleration spectra of the 48 m mid-span under V = 200 km/h

It can be observed from Figs. 8.34, 8.35, 8.36 and 8.37 that:

In the case without collision, the bridge is excited only by the train. For the lateral displacements, the dominant frequency components concentrate on 2.3 and 4.52 Hz (close to 4.12 Hz, the first lateral bending frequency of the bridge) and 6.71 Hz (exactly the second lateral bending frequency). These dominant frequency components are in the range of the natural frequencies, 0.139–7.394 Hz (see Table 8.6), of the ICE3 train vehicle. The spectra for the pier and the mid-span of girder are similar, except that the peak of 6.71 Hz disappeared in the girder's spectrum, as it corresponds to an antisymmetric mode for the girder.

In the case with a collision, a forced vibration occurs simultaneously induced by the train and collision loads. The three types of collision forces are impulsive loads with relatively short duration, so the acting time on the bridge is shorter than that of the train on bridge. During the collision, they excite much larger vibrations than the train, but owing to the damping, the transient vibration excited by the collision attenuates very fast after the collision.

When the collision finishes, it becomes a mixed response composed of the train-induced forced vibration and the free vibration after collision. Therefore, the frequency spectra for vibrations of the bridge simultaneously subjected to train and collision loads are rather complex. Under the ice-I load with several pulses, the dominant frequency of bridge displacement is 1.46 Hz, which is mainly the loading frequency (Fig. 8.29a). Under the ice-II load with shortest pulse and wide frequency band (Fig. 8.29b), the dominant frequency components of bridge displacement are 3.05 Hz (close to 3.35 Hz, the first vertical bending frequency of the bridge) and 6.96 Hz (close to 6.71 Hz, the second lateral bending frequency). This is because the train travels on one track of the bridge with double tracks, which induces a coupled lateral-vertical vibration when the bridge is acted on by a lateral collision. Under the vessel load with a wider continuous pulse, the vibration frequency spectrum shows clearly the quasi-static component, which is mainly due to the quasi-static component of the load (Fig. 8.29c).

For the lateral acceleration responses of the bridge, the frequency spectra are more complex. In the case without collision, the dominant frequencies appear at 2.3, 4.5, and 6.7 Hz for the pier, but again only 2.3 and 4.5 Hz for the girder. Under the collision loads, in addition to the dominant frequencies apparent in the displacement spectra, there appear many peaks at higher frequencies, such as 9.52 Hz for the ice-I load, 10.1 Hz for the ice-II load, and 8.91 Hz for the vessel load, which are close to 9.23 Hz, the third lateral bending frequency of the bridge. Different from the displacement spectra, there is no quasi-static component in any of the acceleration spectra.

To further compare the influence of different collision loads, the maximum lateral displacements and accelerations of the bridge under ice-I load, ice-II load, and vessel load with the collision intensities of 5 MN, 10 MN, and 15 MN are shown in Figs. 8.38, and 8.39, respectively.

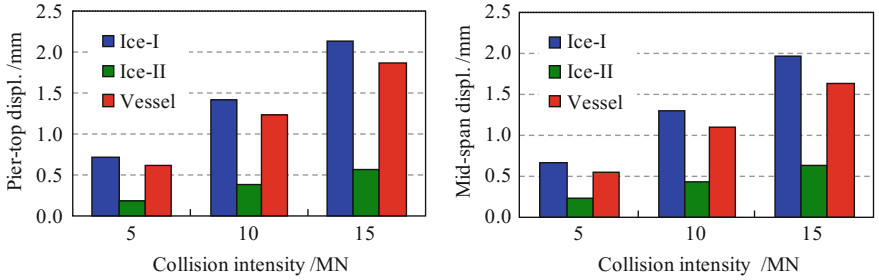

Fig. 8.38 Comparisons of maximum lateral displacements of the bridge at pier-top and mid-span under different collision loads (V = 200 km/h)

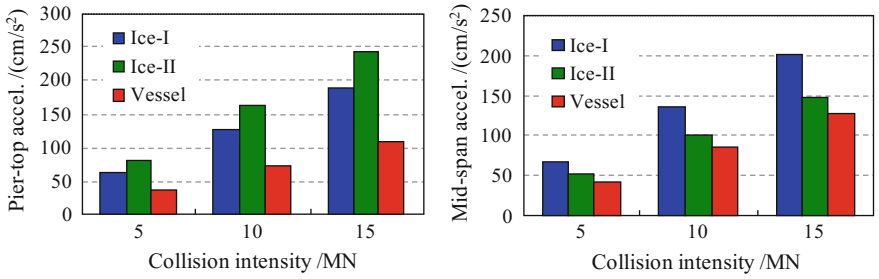

Fig. 8.39 Comparisons of maximum lateral accelerations of the bridge at pier-top and mid-span under different collision loads (V = 200 km/h)

It can be observed from the figures that:

(1) For the collision loads with the same intensity, the maximum displacement of a structure mainly depends on the duration lengths of the loads. From Fig. 8.38, it can be seen that the lateral displacements of the bridge induced by the ice-II load with the shortest duration is the smallest, while the displacements induced by the ice-I load with the longest duration and repeated impacts are bigger than those by the other two collision loads.

(2) The bridge accelerations are mainly influenced by the loading rate of the collision loads. For the three collision loads with the same intensity, the ice-II load with the shortest pulse width (0.06 s) produces the biggest pier-top acceleration and shows the most obvious impact effect. The ice-I load has an obvious peak at its first pulse, which induces a slightly smaller pier-top acceleration than that by the ice-II load. On the other hand, the ice-I load reveals the biggest mid-span acceleration. The accelerations caused by the vessel load, the smallest accelerations, have a relatively steady course, experience a relatively long time to reach their peak, which weakens the impact effect.

8.3.3 *Dynamic Responses of the Train*

Shown in Figs. 8.40, 8.41, and 8.42 are, respectively, the derailment factors, offload factors, and lateral wheel-rail forces of the first car, when the ICE3 train travels on the bridge at V = 200 km/h, without collision and under three collision loads.

It can be seen from the figures that the running safety indices of the train are strongly affected by the collision loads. When the ICE3 train travels on the (32+48+32) m continuous bridge under either of the three collision loads, the derailment factors, offload factors, and lateral wheel-rail forces exhibit obvious difference compared to those without collision. After the impact of collisions, there appear oscillations with large amplitude in the curves, and the peaks of the indices are greatly increased.

Shown in Table 8.5 for comparison are the maximum running safety indices of the train traveling on the bridge at the speed of 200 km/h without collision load and under the three collision loads.

The limits in the table are the criterion for train running safety adopted in the train-bridge coupling dynamic analysis and the joint debugging and commissioning test of Beijing-Shanghai HSR line, namely derailment $Q/P \leq 0.8$, offload factor $\Delta P/P \leq 0.6$, and lateral wheel-rail forces 52.97 kN and 49.08 kN for the motor-car and trailer-car of ICE3 train, corresponding to their static loads of 156.96 kN and 143.22 kN, respectively.

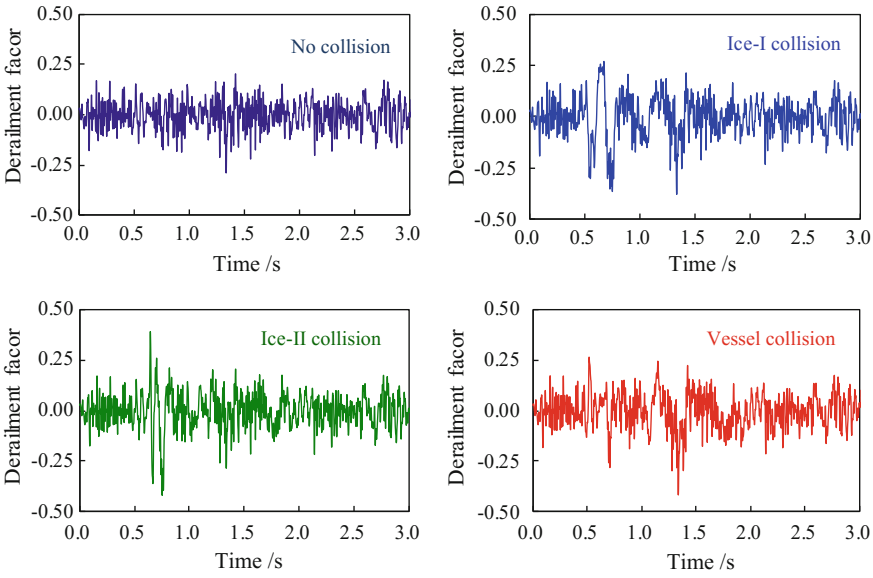

Fig. 8.40 Derailment factor histories of the first car under V = 200 km/h

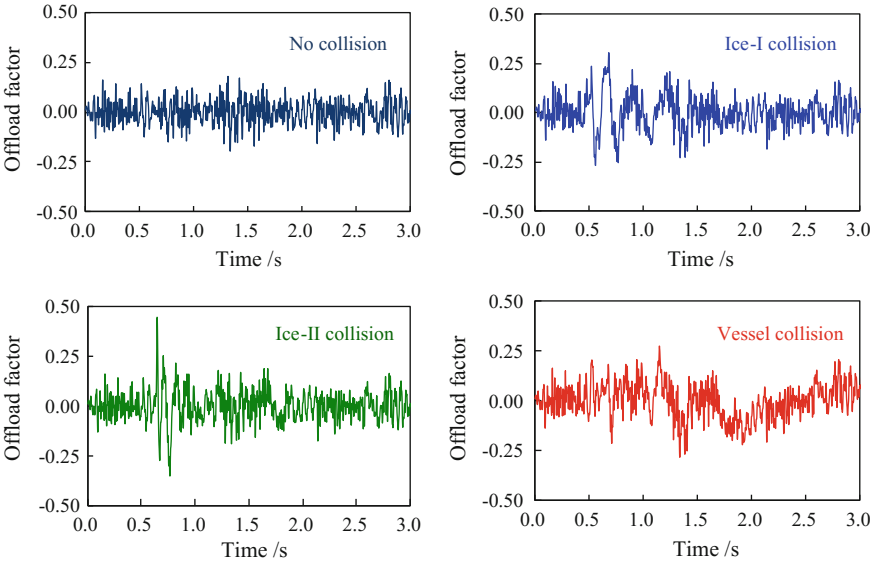

Fig. 8.41 Offload factor histories of the first car under V = 200 km/h

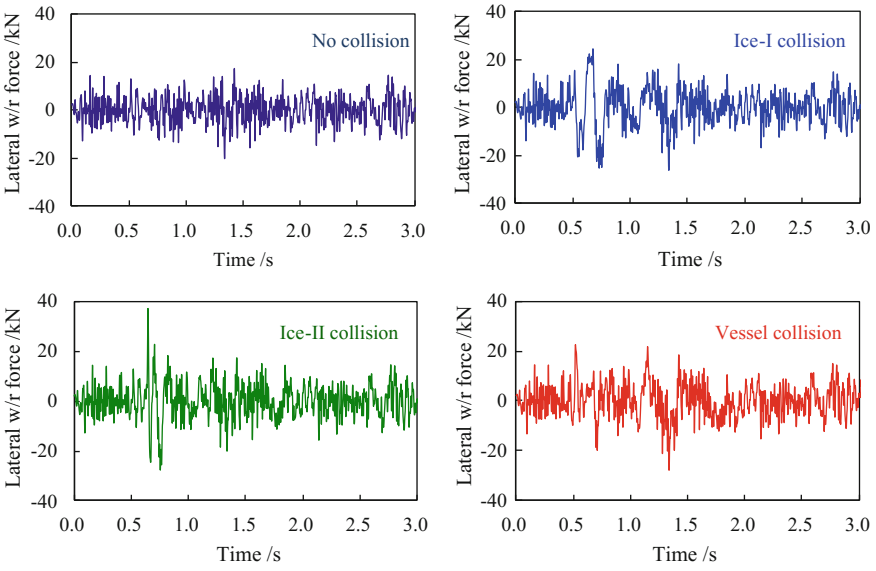

Fig. 8.42 Lateral wheel-rail force histories of the first car under V = 200 km/h

Table 8.5 Maximum running safety indices of ICE3 train on the bridge subjected to various collision loads (V = 200 km/h)

Running safety index		Without collision	With collision loads			Allowance
			Ice-I load	Ice-II load	Vessel load	
Derailment factor Q/P		0.292	0.381	0.424	0.422	0.8
Offload factor ΔP/P		0.196	0.306	0.461	0.293	0.6
Lateral wheel-rail force (kN)	Motor-car	20.535	26.393	37.430	28.110	52.97
	Trailer-car	19.247	20.945	20.046	20.756	49.08

It can be summarized from Figs. 8.40, 8.41, and 8.42, and Table 8.5 that:

(1) There appear strong shock waveforms in the time history curves of the derailment factor, offload factor, and lateral wheel-rail force when the collision load is applied on the bridge. The durations last about 1.5 s, which are shorter than those observed in the bridge responses. For these collision loads, the impact effect induced by the ice-II load is the most intense, indicating that the running safety indices are more influenced by a collision load with a short pulse.
(2) Under the collision loads, the maximum values for the running safety indices are greatly amplified: The derailment factors increase from 0.292 to 0.381 $\sim$ 0.424 by 30.5% $\sim$ 45.2%, the offload factors increase from 0.196 to 0.293 $\sim$ 0.461 by 49.5% $\sim$ 135.2%, and the lateral wheel-rail forces increase from 20.535 to 26.393 $\sim$ 37.43 by 28.5% $\sim$ 82.3%, respectively.
(3) When the bridge is excited by any of the three collision loads with maximum impact force 10 MN, the derailment factor, offload factor, and lateral wheel-rail force of the train running at V = 200 km/h are within the corresponding safety allowances in the Chinese code.

8.4 Influence of Collision Effect on Running Safety of High-Speed Train

The running safety of high-speed trains on railway bridges subjected to collision is an issue of concern in railway engineering. In this section, with the same bridge and track irregularity parameters given in Sect. 8.3.1, the effect of collision on the running safety of train is investigated by considering different train speeds, collision force intensities, and train types. The maximum values of running safety indices, which are taken from the corresponding time histories of all wheel-sets during passage of the train on the bridge, are used for comparison and are evaluated according to the safety evaluation indices.

8.4.1 Influence of Train Speed

While keeping the parameters of the bridge and the ICE3 train unchanged, the train speed is varied from 200 km/h to 320 km/h. The collision intensities are normalized as 5 MN. The curves of maximum derailment factors, offload factors, and lateral wheel-rail forces of motor-car and trailer-car versus train speed are shown in Fig. 8.43, in which the curves related to the "without collision" case have been also included. The horizontal dashed lines represent the related allowance values.

As shown in Fig. 8.43, the increasing tendency of the train running safety indices with the train speed is obvious. Generally, the higher the train speed, the bigger the running safety indices. When the train speed is 320 km/h, the derailment factor under ice-I load exceeds the allowable value, and when the train speed is 350 km/h, the offload factors and lateral wheel-rail forces of trailer-car under all collision loads exceed their related allowances.

8.4.2 Influence of Collision Load Intensity

Using the parameters of the bridge and the ICE3 train and keeping the load shapes and durations unchanged, the influence of collision intensity on the running safety indices is analyzed, by changing the collision intensities from 0 MN to 20 MN. The

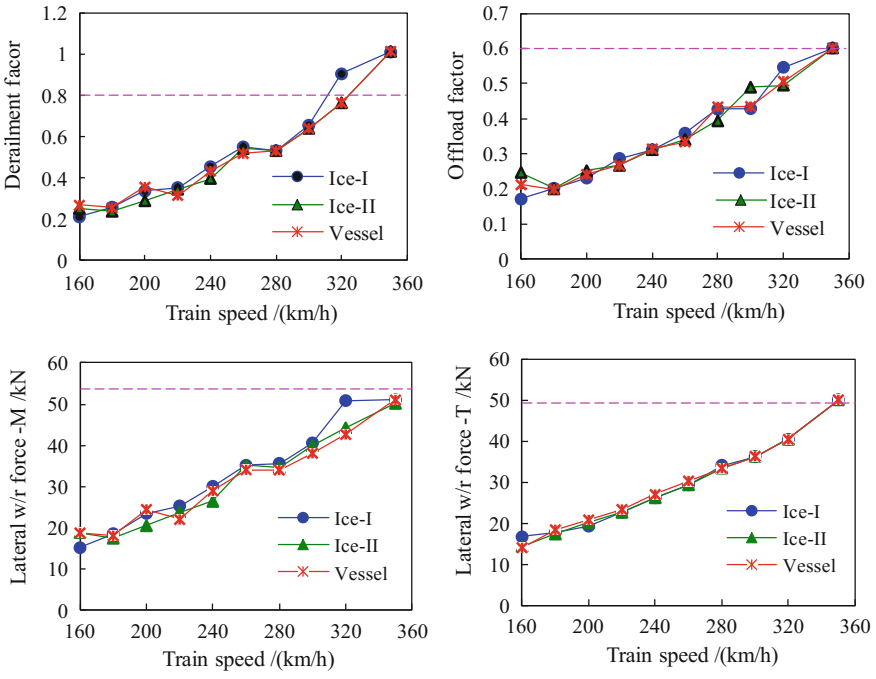

Fig. 8.43 Distributions of running safety indices versus train speed (F_c = 5 MN)

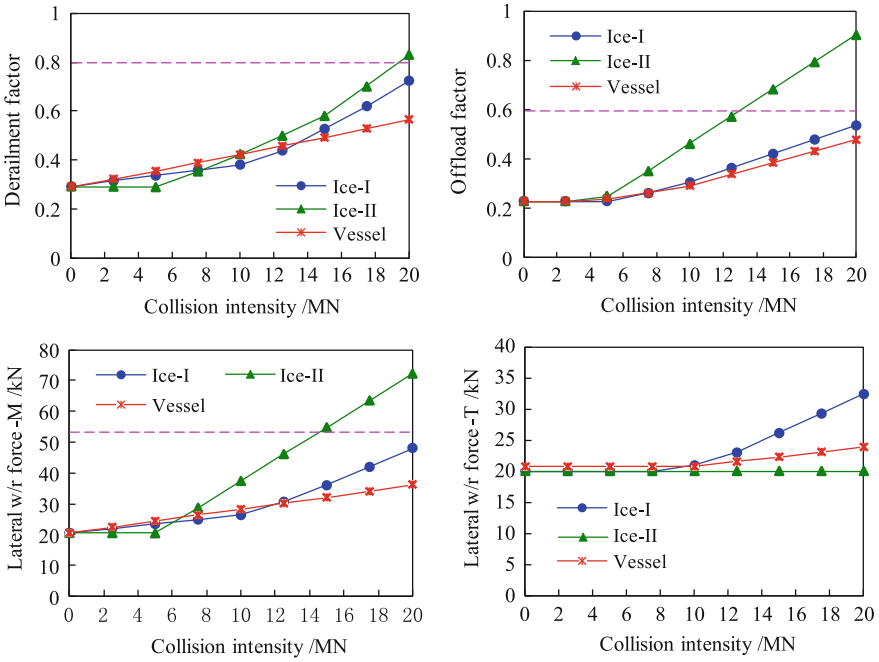

Fig. 8.44 Distributions of running safety indices versus collision intensity (V = 200 km/h)

train speed is 200 km/h. The distribution curves of maximum derailment factors, offload factors, and lateral wheel-rail forces versus collision intensities for the three collision loads are shown in Fig. 8.44, in which the horizontal dashed lines represent the related allowances.

Referring to these figures for the three collisions, the effect of collision intensity on the running safety of the train can be summarized as follows:

(1) The increase of vehicle running safety indices with collision intensity is obvious. Generally, the higher the collision intensity, the bigger the running safety indices, especially when the collision intensity is greater than 5 MN (for the derailment factor, offload factor, and lateral wheel-rail force of motor-car) or 10 MN (for the lateral wheel-rail force of trailer-car).
(2) The influence on the train running safety by the ice-II load with the shortest duration is the most obvious. The ice-I load has a minor influence and the vessel load the smallest.
(3) When the collision intensity of the ice-II load exceeds 15 MN, the offload factor and lateral wheel-rail force of trailer-car exceed the related allowances. For the ice-I load and the vessel load, when the collision intensity is less than 20 MN, the running safety of train can be ensured.

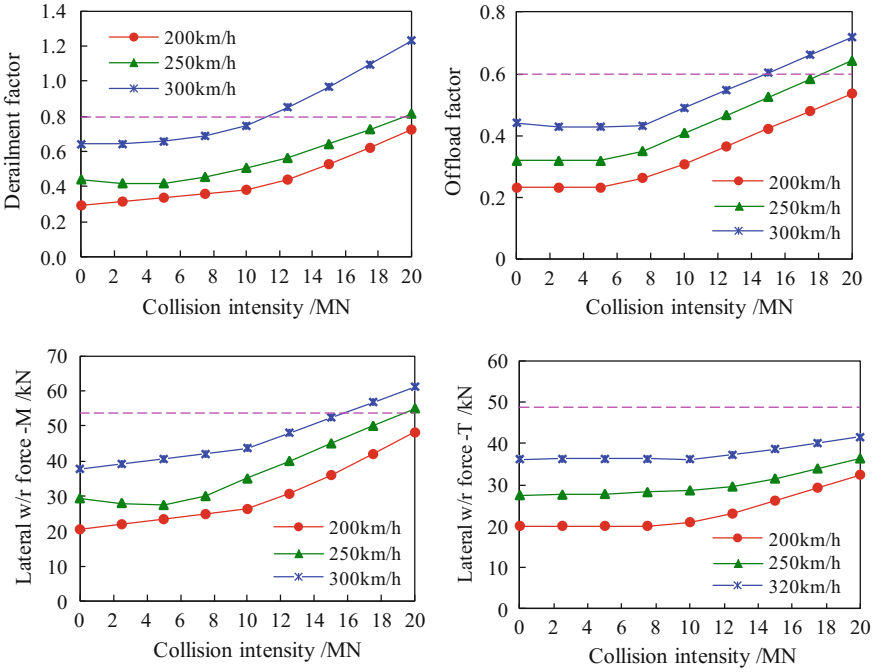

Fig. 8.45 Distributions of running safety indices of ICE3 train versus collision intensity of ice-I load

Shown in Fig. 8.45 are the distribution curves of maximum derailment factors, offload factors, and lateral wheel-rail forces versus collision intensity of the ice-I collision load, by considering three train speeds of 200, 250, and 300 km/h.

From the figures, it can be seen that the distribution curves under the three train speeds have the same tendency: All the train running safety indices increase obviously with the collision intensity. Under the train speed of V = 300 km/h, the derailment factor exceeds the allowance at collision intensity of 12.5 MN, and under V = 250 km/h, the derailment factor, offload factor, and motor-car lateral wheel-rail forces exceed the related allowances at collision intensity of 20 MN.

For better displaying the distributions of running safety indices versus train speed and collision intensity, Fig. 8.46 gives the 3-D graphs. The graphs clearly show how the indices increase with train speed and collision intensity and exceed their safety allowances under certain conditions, to form the respective dangerous zones.

8.4.3 Influence of Train Types

Three types of high-speed trains, Germany ICE3, Japan E500, and China CRH2 with the same composition of 4 × (3 motor-car +1 trailer-car), are considered to analyze the influence of train types on the running safety indices of train vehicles.

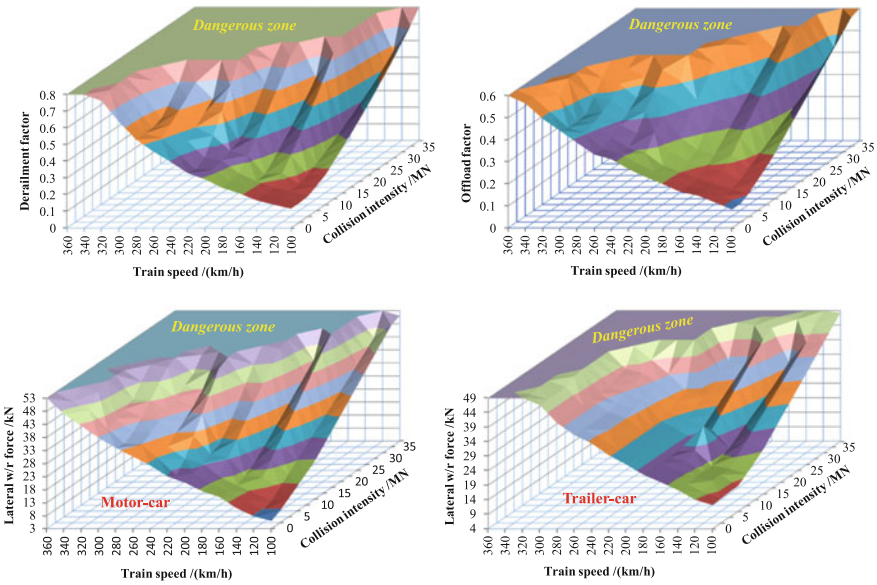

Fig. 8.46 Three-dimensional distribution graphs of train running safety indices versus train speed and collision intensity of ice-I load

For understanding the train-bridge interaction, it is useful to calculate the eigen-frequencies and eigen-modes of the vehicles. Summarized in Table 8.6 are the eigen-frequencies and the corresponding mode shape descriptions of the

Table 8.6 Calculated modal parameters of the train vehicles

Mode description	Frequency (Hz)					
	ICE3		E500		CRH2	
	Motor	Trailer	Motor	Trailer	Motor	Trailer
Vertical movement of car-body	0.588	0.527	0.691	0.730	0.652	0.699
Pitching movement of car-body	0.656	0.568	0.966	0.772	0.937	0.681
Yawing movement of car-body	0.561	0.601	1.126	0.751	0.703	0.704
Lateral-and-rolling movement of car-body, lateral and rolling swings in phase	0.195	0.139	0.437	0.369	0.321	0.381
Lateral-and-rolling movement of car-body, lateral and rolling swings out of phase	0.572	0.641	0.687	0.872	0.805	0.891
Lateral movement of bogie	6.961	7.394	12.765	12.467	10.667	11.834
Vertical movement of bogie	4.396	4.203	4.398	5.621	4.371	4.848

Table 8.7 Allowable values of lateral wheel-rail forces

Type of train	Car type	Static axle load P_{st} (kN)	Allowable lateral wheel-rail force (kN)
Germany ICE3 EMU	Motor	156.96	52.972
	Trailer	143.23	49.082
Japan E500 EMU	Motor	127.53	44.634
	Trailer	134.89	46.718
China CRH2 ENU	Motor	132.44	46.025
	Trailer	117.72	41.854

vehicle. One can find that the three trains have quite different frequencies for all the modes.

The running safety indices for the trains are calculated: For all train types, the allowance values for the derailment and the offload factor are, respectively, 0.8 and 0.6. Owing to the different axle loads of the considered trains, the allowance values for the lateral wheel-rail forces are separately given in Table 8.7.

The ice-I load is adopted with the collision intensities from 0 MN to 20 MN, and the train speed is 200 km/h. Shown in Fig. 8.47 are the curves of the running safety indices for different trains versus collision intensity, in which the dashed, dotted,

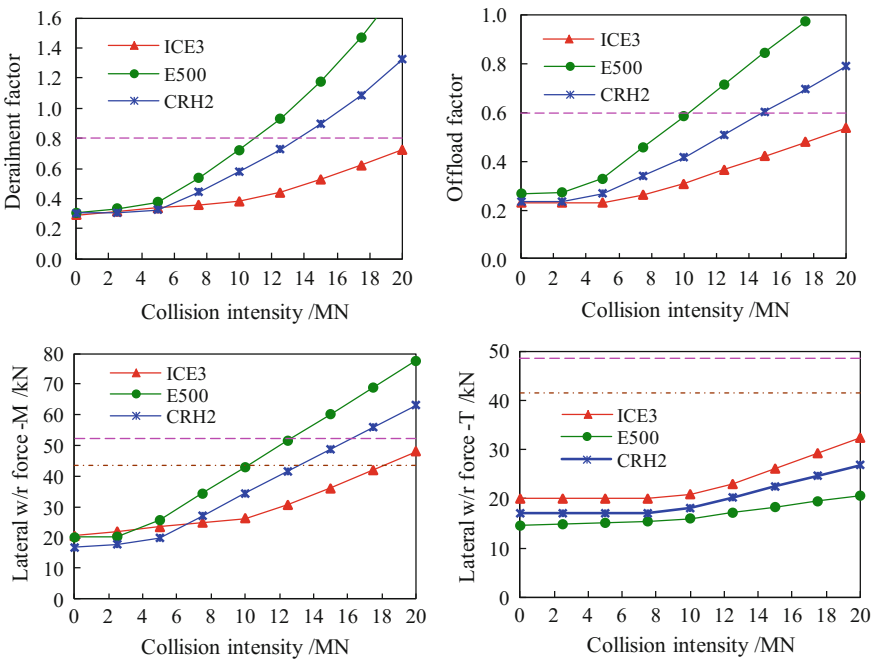

Fig. 8.47 Distributions of running safety indices of different trains versus collision intensity of ice-I load (V = 200 km/h)

and solid horizontal lines represent, respectively, the related allowable values for the ICE3, E500, and CRH2 trains.

Referring to these figures, the influence of train types on the train running safety indices can be summarized as follows:

(1) All the running safety indices of different trains increase with the collision intensity, especially for collision forces bigger than 5 MN.
(2) The influence of collision on the E500 train is the biggest, and the second is on the CRH2 train, while the influence on the ICE3 is the smallest. For the derailment factors, offload factors, and lateral wheel-rail forces, the E500 train exceeds the related allowances when the collision intensity reaches 12.5 MN, and so does the CRH2 train when the collision intensity reaches 15 MN.

Keeping the collision intensity of ice-I load as 5 MN, the running safety indices for ICE3, E500, and CRH2 trains at the speeds of 200 ∼ 350 km/h are calculated, as shown in Fig. 8.48.

As seen in the figures, when the ice-I load is 5 MN, the distributions of running safety indices of three types of trains versus train speed can be summarized as follows:

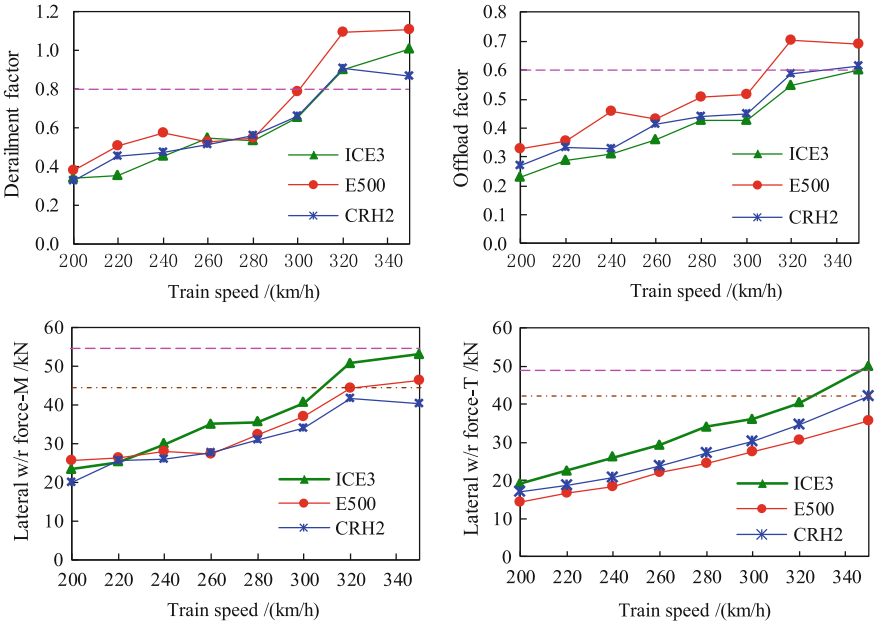

Fig. 8.48 Distributions of running safety indices of different trains versus train speed (ice-I load, F_{max} = 5 MN)

(1) In the main trend, all the indices increase with train speed.
(2) When the train speed reaches 320 km/h, the derailment factors of all the three trains exceed the allowance, and also the offload factor of E500 train. When train speed reaches 350 km/h, the offload factor of CRH2 train exceeds the allowance.
(3) For the train speeds ranged from 200 km/h to 320 km/h, the lateral wheel-rail forces of all the three trains satisfy the allowance. When the train speed reaches 350 km/h, the lateral wheel-rail forces of ICE3 train approaches to or slightly exceeds the allowance.

8.4.4 *Influence of Impulse Form and Duration of Collision Loads*

While keeping the parameters of the bridge and the ICE3 train unchanged, by changing the form and width of the collision load impulse, the derailment factors, offload factors, and lateral wheel-rail forces of ICE3 train are calculated to analyze the influence of impulse form and duration of collision loads on the train running safety. By comprehensively considering the specifications on collision loads in various codes, five types of impulse are adopted for analysis, which are triangular impulse, rectangular impulse, half-sinusoidal impulse, the first impulse of ice-I, and vessel load, as shown in Fig. 8.49. In the figures, F_c is the amplitude, T is the duration, and T_0 is the initial time of the impulse loads.

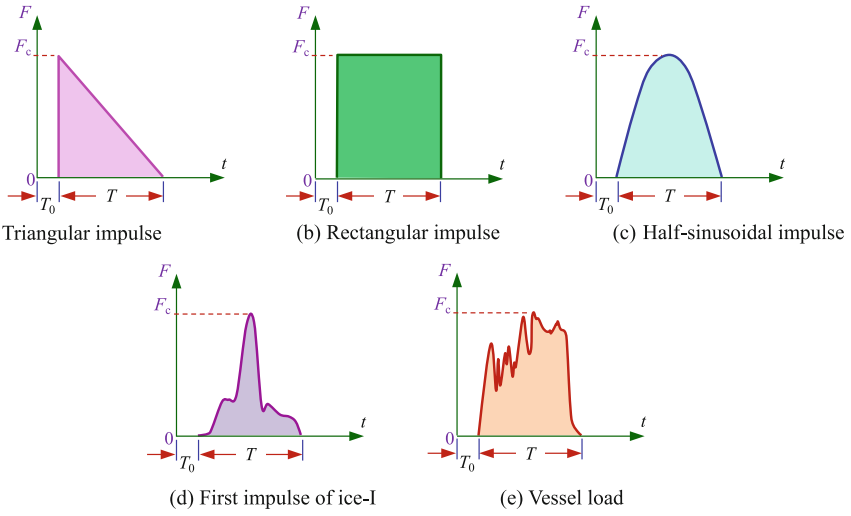

(a) Triangular impulse (b) Rectangular impulse (c) Half-sinusoidal impulse

(d) First impulse of ice-I (e) Vessel load

Fig. 8.49 Waveforms of various impulse loads

Keeping the train speed of 200 km/h and load intensity of 5 MN, the derailment factors, offload factors, and lateral wheel-rail forces of ICE3 train under various collision loads with impulse width 0.05 ~ 5 s are calculated, as shown in Figs. 8.50, 8.51 and 8.52.

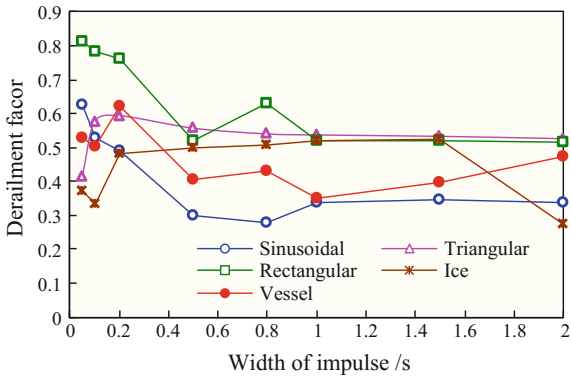

Fig. 8.50 Distributions of derailment factors versus impulse width under various collision loads

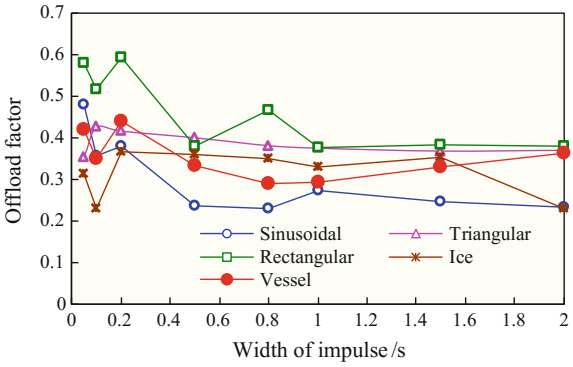

Fig. 8.51 Distributions of offload factors versus impulse width under various collision loads

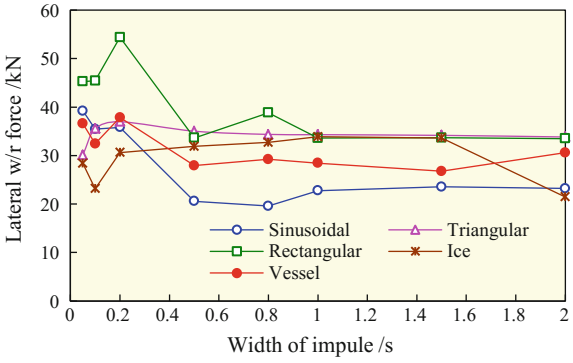

Fig. 8.52 Distributions of lateral wheel-rail forces of motor-car versus impulse width under various collision loads

Referring to these figures, the influence of impulse form and duration of collision loads on the running safety indices of the train can be summarized as follows:

(1) For collision loads with the same duration, the rectangular impulse affects the train running safety most, because it loads on and unloads from the pier as a step function with the most fast loading rate. For the triangular impulse, it loads on the pier as a step form but unloads gradually, so it has smaller effect.
(2) With the decrease of pulse width, the influence on train running safety is enlarged. For the rectangular impulse load less than 0.2 s (smaller than the fundamental natural period of the bridge, i.e., 0.24 s), the interval between loading and unloading is very short, so the impact effect is the most obvious, when the derailment factor, offload factor, and lateral wheel-rail force of ICE3 train approach to or exceed the allowances.
(3) In the five loads, the first impulse of ice-I load has the lowest loading rate, so when the impulse width is less than 0.2 s, its effect on train running safety is the smallest.
(4) In general, short impulsive loads (especially when $T < 0.2$ s) have more influence on the train running safety. When $T > 1.0$ s, the indices change little with impulse width.

8.5 A Framework for Running Safety Assessment of High-Speed Train on Bridge Subjected to Collision Loads

The previous analyses show that the running safety indices of the train are influenced by the types and intensities of the collision loads, and also the types and the speeds of the trains. To ensure the running safety of trains on bridges subjected to collision loads, a further simulation is performed to find out an assessment method and the corresponding thresholds.

8.5.1 Analysis Method

Collision intensity and train speed are the two main factors affecting the running safety of train. The threshold speed of trains can be determined according to the safety evaluation indices in the following way:

(1) Keeping the collision intensity as a constant at each stage, the dynamic responses of the train are calculated by changing the train speed from 100 km/h to 360 km/h with an increment of 20 km/h. The running safety indices (derailment factors, offload factors, and lateral wheel-rail forces) are calculated and compared with the related allowances. If any of these allowances is

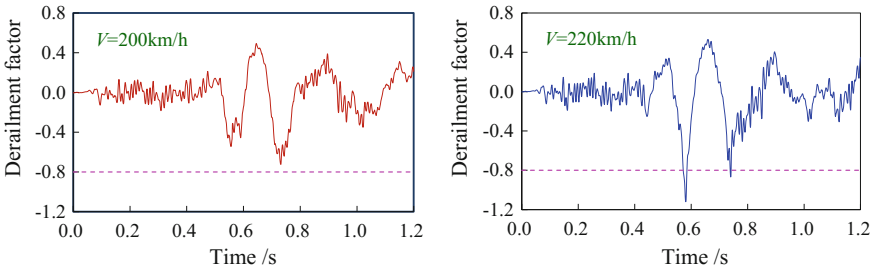

Fig. 8.53 Determination of the critical train speed for train running safety corresponding to a collision intensity of 20 MN

exceeded, the previous lower train speed is considered as the critical train speed for the corresponding collision intensity.

For example, as shown in Fig. 8.53, corresponding to the ice-I load with the intensity of 20 MN, the derailment factor of the train at V = 200 km/h is 0.724, which meets the allowance value of 0.8 (the dashed line in the figure). While at V = 220 km/h, the derailment factor increases to 1.119, which exceeds the allowance. At this time, no matter whether the offload factor and the lateral wheel-rail force exceed the related allowance values or not, V = 200 km/h is regarded as the critical train speed corresponding to the collision intensity of 20 MN.

(2) Then, the collision intensity is changed from 0 MN (no collision) with an increment of 2.5 MN. For each kind of collision intensity, the dynamic responses of the train vehicles are calculated at different train speeds. In this way, the critical train speeds related to all collision intensities considered are acquired.

Herein, the analysis is limited to the case where the bridge produces strong vibration but is not damaged when it is subjected to collision. Therefore, the collision intensity is limited to 40 MN for this bridge, to ensure the structure can still work in the elastic stage.

8.5.2 Threshold Curves for Running Safety of ICE3 Train on the Bridge Subjected to Ice-I Collision Load

The procedure to determine the threshold curves for train running safety is illustrated by using the continuous bridge, the ICE3 train, and the ice-I collision load as an example. The maximum values of running safety indices are calculated, in the case of the train travelling at different speeds on the bridge subjected to collision loads with different intensities. The results for the derailment factors are listed in Table 8.8.

Table 8.8 Maximum derailment factors with different train speeds and collision intensities

Train speed (km/h)	Collision intensity (MN)															
	0	2.5	5	7.5	10	12.5	15	17.5	20	22.5	25	27.5	30	32.5	35	37.5
100	0.116	0.116	0.121	0.148	0.176	0.222	0.269	0.318	0.369	0.422	0.478	0.536	0.596	0.659	0.726	*0.869*
120	0.140	0.144	0.152	0.16	0.18	0.211	0.243	0.277	0.313	0.349	0.387	0.427	0.467	0.517	0.569	
140	0.166	0.166	0.172	0.223	0.295	0.372	0.453	0.541	0.634	0.734	*0.841*	*0.956*	*1.079*	*1.213*	*1.357*	
160	0.208	0.210	0.211	0.216	0.270	0.327	0.387	0.450	0.517	0.589						
180	0.242	0.250	0.258	0.331	0.407	0.486	0.570	0.657	0.748	*0.856*						
200	0.292	0.314	0.336	0.358	0.381	0.439	0.527	0.620	0.724							
220	0.330	0.315	0.353	0.449	0.560	0.681	*0.813*	*0.959*	*1.119*							
240	0.398	0.407	0.454	0.501	0.550	0.600										
260	0.460	0.504	0.550	0.597	0.647	0.698										
280	0.532	0.532	0.532	0.553	0.618	0.686										
300	0.640	0.641	0.655	0.688	0.745	*0.852*										
320	0.764	0.793	*0.904*	*0.904*	*1.023*											
340	*0.895*	*0.895*														

It can be noticed that the maximum derailment factor increases with the train speed in general for each collision intensity, and it will exceed the allowance of 0.8 when the train speed reaches a certain value. The train speed at the previous lower level is regarded as the critical train speed corresponding to this collision intensity. Similar tables can be obtained for the offload factors and the lateral wheel-rail forces.

By plotting the calculated results in a coordinate system, with the abscissa representing the collision intensity and the ordinate the train speed, a group of relationship curves between the critical train speed and the collision intensity can be obtained, as shown in Fig. 8.54. The curves define the boundary of safety zones for the high-speed train on the bridge subjected to collision with various intensities, corresponding to the derailment factors, offload factor, and lateral wheel-rail forces of motor-car and trailer-car, respectively.

The curve in each figure divides the whole zone into two parts. In the lower left zone, the running safety index meets the related allowance given in Table 8.5, indicating that the running safety of the train can be ensured, while in the upper right zone, the index exceeds the related allowance, indicating that the running safety of the train cannot be guaranteed.

Furthermore, the lowest critical train speeds for different collision intensities are connected, forming an inscribed curve, as the thick line shown in Fig. 8.55. This inscribed curve divides the whole zone into two parts. In the lower left zone, all the running safety indices meet the related allowances, indicating that the running safety of the train is ensured, while in the upper right zone, at least one of the

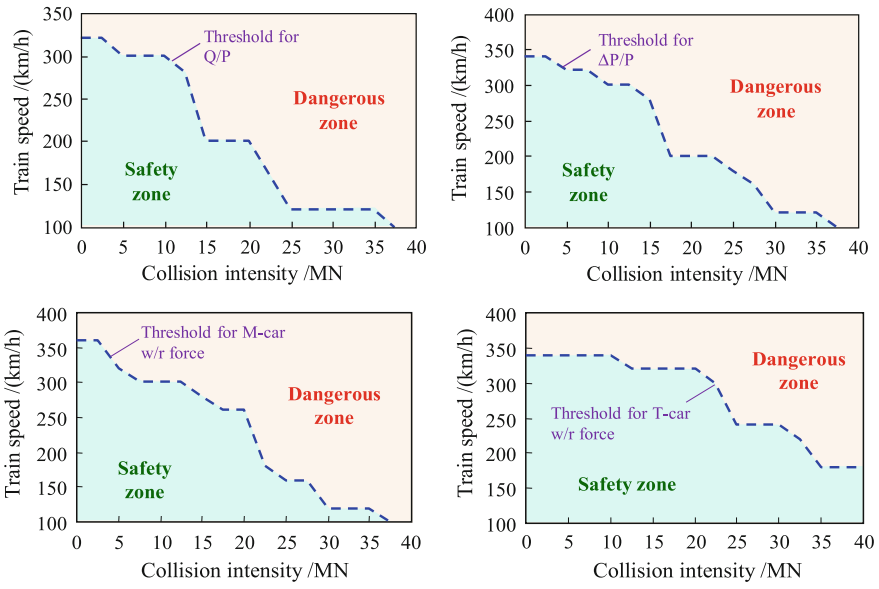

Fig. 8.54 Threshold curves of train speed versus impact intensity for running safety of ICE3

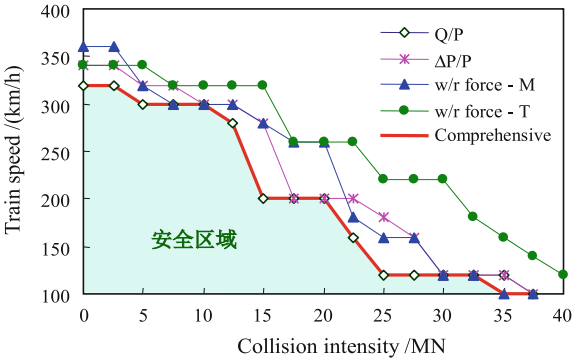

Fig. 8.55 Threshold curves of train speed versus impact intensity for running safety of ICE3 train considering ice-I collision loads

indices exceeds the related allowance, indicating that the running safety of the train cannot be guaranteed.

From the figure, it can be observed that the running safety indices of the train are influenced comprehensively by the collision intensity and the train speed.

(1) The greater the collision intensity, the lower the allowable train speed for running safety. In the case without collision load, all indices meet the related allowances for the train speed up to 320 km/h. With the increase of collision intensity, the train should gradually lower its speed to ensure the running safety. When the collision intensity reaches 35 MN, the train can only run safely at the speed of 100 km/h.

(2) The higher the train speed, the smaller the collision intensity that the train-bridge system can sustain. At V = 200 km/h, the train can run safely for a collision intensity up to 20 MN; at V = 250 km/h, the allowable collision intensity is lowered to less than 15 MN; while at V = 300 km/h, only 5 MN collision intensity is allowed to ensure the train running safety.

8.5.3 Comparison of Running Safety Thresholds for Different Collision Loads

Some bridges may suffer different types of collision loads. For example, for a bridge across a river that freezes in winter while it is open to navigation in summer, it may be collided by a vessel in summer as well as by ice-floes in early spring. Considering this case, the running safety threshold curves for the ice-II load and vessel load are also obtained in a similar way, and the three curves are plotted in a same figure, as shown in Fig. 8.56.

Because the different collisions do not happen at the same time, a comprehensive threshold curve for running safety of the ICE3 train is acquired, which is the inscribed curve that connects the lowest critical train speeds for each of the three collision loads, as the thick line shown in the figure.

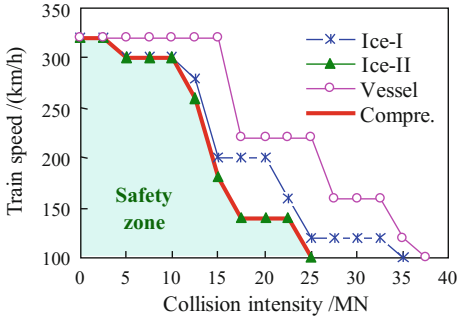

Fig. 8.56 Threshold curves of train speed versus impact intensity for running safety of ICE3 train under various collision loads

From all three collision loads, the ice-II load has the biggest influence on the running safety of the ICE3 train. For example, for the vessel load of 15 MN, the safety train speed is V = 320 km/h, for the ice-I load, it is lowered to 200 km/h, while for the ice-II load, the train can only run safely at 180 km/h. Thus, the boundary of safety zone is decided mainly by the ice-II load.

Comprehensively considering three types of loads, when the collision intensity F_c = 15 MN, the running safety of the ICE3 train at the speeds of 200 km/h and 250 km/h will be affected; while when F_c = 10 MN, the speed limit for ICE3 train will be 300 km/h.

8.5.4 *Comparison of Running Safety Thresholds for Different Trains*

Similar to Fig. 8.56 for the ICE3 train, the threshold curves can be obtained for the E500 and CRH2 trains, as shown in Fig. 8.57, to study the effects of collision on different types of high-speed trains.

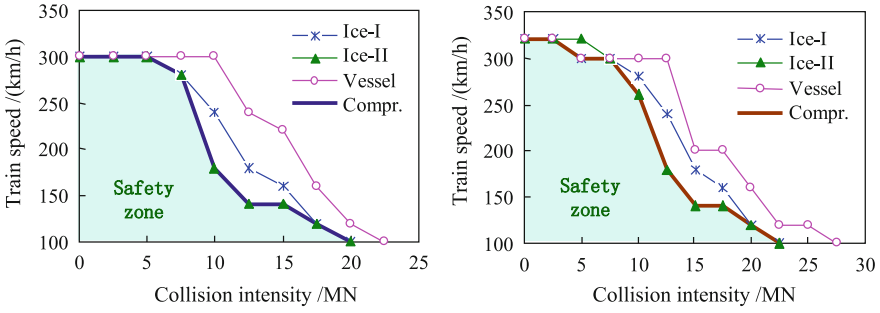

Fig. 8.57 Threshold curves of train speed versus impact intensity for running safety of E500 and CRH2 trains under various collision loads

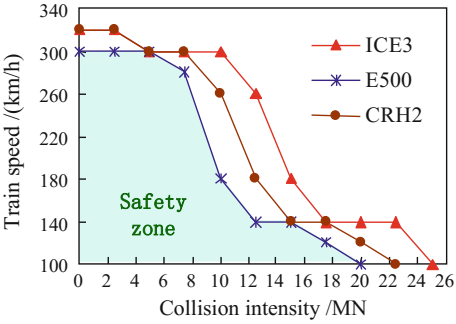

Fig. 8.58 Comparison of running safety threshold curves for different trains

It is observed from Figs. 8.56 and 8.57 that obvious differences exist between the threshold curves for different trains. Comparatively for the three trains, the ice-II load has the biggest influence on the running safety of the trains. This is especially true for the ICE3 and E500 trains where the threshold curves are completely determined by the ice-II load.

The comprehensive threshold curves for the three trains (the inscribed curves in Figs. 8.56 and 8.57) are resumed in Fig. 8.58.

Referring to the figure, the influence of train types on the running safety of trains can be summarized as follows:

(1) With the increase of collision intensity, the train has to lower its speed to ensure the running safety. For example, the safety train speed for E500 is 300 km/h for the collision intensity up to 5 MN, and it is 280 km/h for the collision intensity of 7.5 MN, while it can only run at a speed lower than 200 km/h when the collision intensity is 10 MN.

(2) Considering all three collision loads, the running safety threshold curves for the three trains show the same tendency: E500 is the most sensitive to collision, CRH2 is the second, and ICE3 is the less sensitive. For example, the E500 can run safely at 300 km/h when no collision is applied on the bridge. When the collision intensity reaches to 20 MN, the safe train speed of E500 is lowered to 100 km/h, while under the same intensity, CRH2 can run at 120 m/h and ICE3 at 140 km/h. Only when the collision intensities reach to 22.5 MN and 25 MN, the safe running speeds of CRH2 and ICE3 trains reduce to 100 km/h.

(3) From the above analysis and referring to Tables 8.7 and 8.8, one can notice that for the three types of trains, E500 has the lightest axle load and the highest natural frequencies (especially those of the bogies), while ICE3 has the heaviest axle load and the lowest natural frequencies. For a train vehicle, higher frequency of the bogie usually means larger suspension stiffness between the bogie and the wheel-sets, so it can be concluded that the running safety of the train with smaller axle load and larger suspension stiffness is more easily influenced when the bridge is collided.

8.6 Conclusions

The following conclusions can be drawn from the case study:

(1) A collision load has an obvious effect on the dynamic responses of the bridge. The lateral displacement and acceleration responses of the bridge subjected to a collision are much greater than the ones without collision. The lateral displacement of the bridge is more influenced by a collision load with a long pulse related to the natural period of the bridge, while the acceleration is more influenced by a load with a short pulse and a fast loading rate.
(2) Vibrations induced by collision loads have a great effect on the dynamic responses of high-speed trains. The running safety of the train is affected by both the type and intensity of the collision load acting on the bridge, and the type and running speed of the train. Strong collision may threaten the running safety of high-speed trains. Generally, the greater the collision intensity and the higher the train speed, the bigger the influence of collision on the running safety of the train. The running safety of the train can be evaluated by the threshold curve between train speeds and collision intensities.
(3) For the high-speed train on the bridge, the running safety indices are mainly influenced by the peak value and the width of the pulse of the collision load. The pulse with short duration time and fast loading rate has a bigger influence than the pulse with long duration time and slow loading rate.
(4) The sensitivities of the running safety indices to a collision are dependent on train type. The running safety of the train with lighter axle loads and larger suspension stiffness is more easily affected when the bridge is collided.
(5) The proposed methodology may provide a reference for the dynamic design of railway bridges.

Dynamic analysis of coupled train-bridge systems subjected to collision loads is a rather complex problem, which is related to the running speed of the train, the structural form of the bridge, the intensity, and acting position of the collision load, and many other factors. In this paper, only a preliminary study is performed and illustrated by a case study. The proposed analysis framework and the calculation results may provide a reference for the dynamic design of high-speed railway bridges subjected to vessel collision.

Moreover, in this study, only the case was considered where the bridge produced strong vibration but not damaged when it was subjected to a collision. When the structure is damaged by the collision, the structure may produce plastic deformation, which may not only change the structural properties of the bridge, but also seriously influence the profile of the track on the bridge, inducing a direct derailment risk of the train. This situation is much more complicated and will be considered in the future study.

References

AASHTO (1991) Guide specifications and commentary for vessel collision design of highway bridges (GVCB-2-2009) [S]. American Association of State Highway and Transportation Officials, Washington, D.C

AASHTO (2007) LRFD bridge design specifications [S]. American Association of State Highway and Transportation Officials, Washington, D.C

British Standard (2006) BS EN1991-1-7: Eurocode 1—actions on structures general action: accidental actions [S]

Buth CE (2009) Guidelines for designing bridge piers and abutments for vehicle collisions-semi annual report [S]. Texas Transportation Institute, College Station, TX, USA

Chen C (2006) Simulation research on design ship collision force and damage state of bridge [D]. Yongji University, Shanghai (in Chinese)

Chen XD, Jin XL, Du XG (2008) Simulation analysis of ship-bridge collision based on parallel algorithm [J]. J Vib Shock 27(9):82–86

Consolazio GR, Chung JH, Gurley KR (2003) Impact simulation and full-scale crash testing of a low profile concrete work zone barrier [J]. Comput Struct 81(13):1359–1374

Derucher KN (1984) Bridge pile damage upon vessel impact [J]. Comput Struct 18(5):931–935

Dong JW, Li ZJ, Lu P et al (2012) Design ice load for piles subjected to ice impact [J]. Cold Reg Sci Technol 71(2):34–43

EL-Tawil S, Severino E, Fonseca P (2005) Vehicle collision with bridge piers [J]. J Bridge Eng 10 (3):345–353

European Standard (1991) Eurocode EN1991-1-7: Actions Sur les Structures Partie 1-7: Actions Générales - Actions Accidentelles [S]. Comité Européen de Normalisation

Fan W, Yuan WC (2012) Shock spectrum analysis method for dynamic demand of bridge structures subjected to barge collisions [J]. Comput Struct 90–91:1–12

Guo FW (2010) Analysis of squeezing ice load of vertical structure based on experimental data [D]. Dalian University of Science and Technology, Dalian (in Chinese)

Han Y (2000) Study on calculation method of river ice to bridge pier structure [D]. Harbin University of Civil Engineering and Architecture, Harbin (in Chinese)

He HQ (2004) Finite element simulation of vessel-bridge collision [D]. Yongji University, Shanghai (in Chinese)

He ZX (2008) Study on some mechanical problems in the damage and destruction of road and bridge [D]. Taiyuan University of Science and Technology, Taiyuan (in Chinese)

Hu ZQ, Gu YN, Gao Z, Li YN (2005) Fast evaluation of ship-bridge collision force based on nonlinear numerical simulation [J]. Eng Mech 22(3):235–240 (in Chinese)

JTG D60 (2015) General specifications for design of highway bridges and culverts [S]. Ministry of communications of PRC. People's Communications Press, Beijing (in Chinese)

Laigaard JJ, Svensson E, Ennemark E (1996) Ship-induced derailment on a railway bridge [J]. Struct Eng Int 6(2):107–112

Li SY, Wang SG, Liu WQ et al (2006) Numerical simulations of ship collision with protective devices of bridge pier [J]. J Nat Disasters 15(5):100–106 (in Chinese)

Liu Y (2011) Numerical simulation of dynamic ice action on cross-sea bridge foundation [C]. In: 2nd international conference on mechanic automation and control engineering, MACE, pp 6625–6628

Lu XZ, He YT, Huang SN (2011) Collision between over-height vehicles and bridge superstructures: failure mechanism, design methodology and protective measures [M]. China Architecture and Building Press, Beijing (in Chinese)

Luo L (2008) Study on vessel-bridge collision theory and performance of anti-collision device on the liede bridge [D]. Changsha University of Science and Technology, Changsha (in Chinese)

Larry D, Olson PE (2005) Dynamic bridge substructure evaluation and monitoring [R]. Report No. FHWA-RD-03-089, US Federal Highway Administration

Manen SE (2001) Ship collision due to the presence of bridges [S]. Technical Report, PIANC General Secretariat, Brussels

Manuel L, Kallivokas LF, Williamson EB et al (2006) A probabilistic analysis of the frequency of bridge collapses due to vessel impact [R]. CTR Technical Report: 0-4650-1

NCAC (2010) Finite element model archive [OL]. http://www.ncac.gwu.edu/vml/models.html

Sharma H, Hurlebaus S, Gardoni P (2012) Performance-based response evaluation of reinforced concrete columns subject to vehicle impact [J]. Int J Impact Eng 43(5):52–62

TB10002.1 (2005) Fundamental code for design on railway bridge and culvert [S]. China Railway Press, Beijing

TB10621-2014 (2015) Code for design of high-speed railway [S]. China Railway Press, Beijing

Thilakarathna HMI, Thambiratnam DP, Dhanasekar M, Perera N (2010) Numerical simulation of axially loaded concrete columns under transverse impact and vulnerability assessment [J]. Int J Impact Eng 37(11):1100–1112

Timco GW, Johnston M (2003) Ice loads on the Molikpaq in the Canadian Beaufort Sea [J]. Cold Reg Sci Technol 37(2):51–68

Timco GW (2011) Isolated ice floe impacts [J]. Cold Reg Sci Technol 68(2):35–48

Tuhkuri J (1995) Experimental observations of the brittle failure process of ice and ice-structure contact [J]. Cold Reg Sci Technol 23:265–278

Wang JJ, Chen C (2007) Simulation of damage for bridge pier subjected to ship impact [J]. Eng Mech 24(7):156–160 (in Chinese)

Wang JJ, Yan HQ, Qian Y (2006) Comparisons of design formula of ship collision for bridges based on FEM simulations [J]. J Highw Transp Res Dev 23(2):68–73

Wang LL, Yang LM, Huang DJ, Zhang ZW, Chen GY (2008) An impact dynamics analysis on a new crashworthy device against ship–bridge collision [J]. Int J Impact Eng 35(8):895–904

Wuttrich R, Wekezer J, Yazdani N, Wilson C (2001) Performance evaluation of existing bridge fenders for ship impact [J]. J Perform Constr Facil ASCE 15(1):17–23

Wu WH, Yu BJ, Xu N, Yue QJ (2008) Numerical simulation of dynamic ice action on conical structure [J]. Eng Mech 25(11):192–196 (in Chinese)

Xia CY (2012a) Dynamic responses of train-bridge system subjected to collision loads and running safety evaluation of high-speed trains [D]. Beijing Jiaotong University, Beijing (in Chinese)

Xia CY, Lei JQ, Zhang N et al (2012b) Dynamic analysis of a coupled high-speed train and bridge system subjected to collision load [J]. J Sound Vib 331(10):2334–2347

Xia CY, Xia H, Zhang N et al (2013) Effect of truck collision on the dynamic response of train-bridge systems and running safety of high-speed trains [J]. Int J Struct Stab Dyn 13(3):1–18

Xia CY, Xia H, De Roeck G (2014) Dynamic response of a train-bridge system under collision loads and running safety evaluation of high-speed trains [J]. Comput Struct 140:23–28

Xia CY, Ma J, Xia H (2015) Dynamic analysis of a train-bridge system to vessel collision and running safety of high-speed trains [J]. Vibroengineering PROCEDIA 5:509–514

Xia CY, Zhang N, Xia H, Ma Q, Wu X (2016) A framework for carrying out train safety evaluation and vibration analysis of a trussed-arch bridge subjected to vessel collision [J]. Struct Eng Mech 59(4):683–701

Xia H, De Roeck G, Goicolea JM (2011) Bridge vibration and controls: new research [M]. Nova Science Publishers, New York

Xu LJ, Lu XZ, Smith ST et al (2012) Scaled model test for collision between over-height truck and bridge superstructure [J]. Int J Impact Eng 49:31–42

Xu LJ, Lu XZ, Guan H, Zhang YS (2013) Finite element and simplified models for collision simulation between over-height trucks and bridge superstructures [J]. J Bridge Eng ASCE 18 (11):1140–1151

Xuan Y, Zhang D (2001) Derailment of train caused by collision between ships and railway bridge pier [J]. Foreign Bridges 4:60–64 (in Chinese)

Yan HQ (2006) Simulation of damage and impact forces for bridge piers subjected to ship collision [D]. Tongji University, Shanghai (in Chinese)

Yu M, Zha XX (2011) Behavior of solid and hollow concrete filled steel tube columns under vehicle impact [J]. Prog Steel Build Struct 13(1):57–64

Yu TL, Yuan ZG, Huang ML (2009a) Experiment research on mechanical behavior of river ice [C]. In: Proceedings of the 19th international symposium on ice, Vancouver, pp 519–530

Yue QJ, Guo FW, Kärnä T (2009b) Dynamic ice forces of slender vertical structures due to ice crushing [J]. Cold Reg Sci Technol 56(2–3):77–83

Zhang YL, Lin G, Li ZJ et al (2002) Application of DDA approach to simulate ice-breaking process and evaluate ice force exerting on the structure [J]. China Ocean Eng 16(3):273–282 (in Chinese)